Clinica Chimica Acta 504 (2020) 43–55

Contents lists available at ScienceDirect

Clinica Chimica Acta

journal homepage: www.elsevier.com/locate/cca

Review

Advances in prostate specific antigen biosensors-impact of nanotechnology

M. Negahdary[a], N. Sattarahmady[a,b,*], H. Heli[a,*]

[a] Nanomedicine and Nanobiology Research Center, Shiraz University of Medical Sciences, Shiraz, Iran
[b] Department of Medical Physics, School of Medicine, Shiraz University of Medical Sciences, Shiraz, Iran

ARTICLE INFO

Keywords:
Prostate specific antigen
Immunosensing
Aptasensor
Peptide-based biosensor
Nanomaterials

ABSTRACT

Prostate cancer is one of the most dangerous and deadly cancers in elderly men. Early diagnosis using prostate-specific antigen (PSA) facilitates disease detection, management and treatment. Biosensors have recently been used as sensitive, selective, inexpensive and rapid diagnostic tools for PSA detection. In this review, a variety of PSA biosensors such as aptasensors, peptisensors and immunesensors are highlighted. These use aptamers, peptides and antibodies in the biorecognition element, respectively, and can detect PSA with very high sensitivity via electrochemical, electrochemiluminescence, fluorescence and surface-enhanced Raman spectroscopy. To improve the sensitivity of most of these PSA biosensors, different nanostructured materials have played a critical role.

1. Introduction

Prostate cancer, as one of the most common diseases, is considered as a major cause of death in men [1,2]. Prostate-specific antigen (PSA), a serine protease, is the most important, reliable and preferred biomarker for early diagnosis of prostate cancer [3,4]. PSA is secreted from normal prostate glandular cells and prostate cancer cells [5]. This glycoprotein biomarker (33–34 KDa) is also known as kallikrein-3 and can be used for evaluating healthy individuals or patients wherein normal serum concentration should be lower than 4 ng mL^{-1} (cutoff value) in men. When prostate cancer occurs, this biomarker increases in serum. In addition to prostate cancerous cells, this biomarker also increases in breast cancer (with a median level of 0.31 ng mL^{-1}). Early detection of prostate cancer through clinical and novel bioanalysis platforms will impact survival. Therefore, finding improved diagnostic tools with high selectivity, sensitivity and stability is necessary. Up to now, several antibody-based methods such as radioimmunoassay [6], enzyme-linked immunosorbent assay (ELISA) [7], surface plasmon resonance (SPR) immunoassay [8] and fluorescence immunoassay [9] have been used for detection of this biomarker. The most important limitations of these methods include high cost, complicated technology, limitations of laboratory tests, lack of portable devices and role of interfering factors. On the other hand, biosensors are designed and produced with lower costs and can detect appropriate analytes with high sensitivity and specificity [3,10].

An increased ratio of surface area to volume and introducing special physicochemical properties including higher (re)activity and quantum behaviors have led to huge applications of nanostructured materials in design of the biosensor transducers. Nanostructured materials (i) increase the surface area of the transducer leading to higher surface concentration of the biorecognition element; (ii) provide more successful and stable immobilization of the biorecognition element on the transducer surface [11,12]; (iii) participate in the detection process through conjugation with the biorecognition element [13,14]; (iv) change the way to generate the output signal [15,16]; (v) represent synergism effects (e.g. when employed as nanocomposites); (vi) are employed as tags or labels [14,17,18]; and (vii) provide multiple analyte detection [19]. These factors lead to amplified signals generation followed by an increment in sensitivity and selectivity [20,21].

The biosensors have hitherto been reported for the detection of PSA and are categorized as aptamer- (aptasensors), peptide- (peptisensors) and antibody-based (immunosensors) biosensors. Based on the type of biorecognition element, the PSA biosensors are discussed in the following part. The main details of each designed biosensor are also provided in several tables. The results of this review may be considered to define new related researches, applicable for the production of commercial PSA diagnosis devices and also can provide optimized experimental procedures for early diagnosis of prostate cancer.

2. PSA aptasensors

For diagnosis, aptamers have several advantages over antibodies such as in vitro production, smaller size, reversible conformation against temperature changes, non-immunogenicity, functionalization

* Corresponding authors at: Nanomedicine and Nanobiology Research Center, Shiraz University of Medical Sciences, Shiraz, Iran (N. Sattarahmady).
E-mail addresses: nsattar@sums.ac.ir, sattarahmady@yahoo.com (N. Sattarahmady), heli@sums.ac.ir, hheli7@yahoo.com (H. Heli).

https://doi.org/10.1016/j.cca.2020.01.028
Received 3 December 2019; Received in revised form 25 January 2020; Accepted 27 January 2020
Available online 28 January 2020

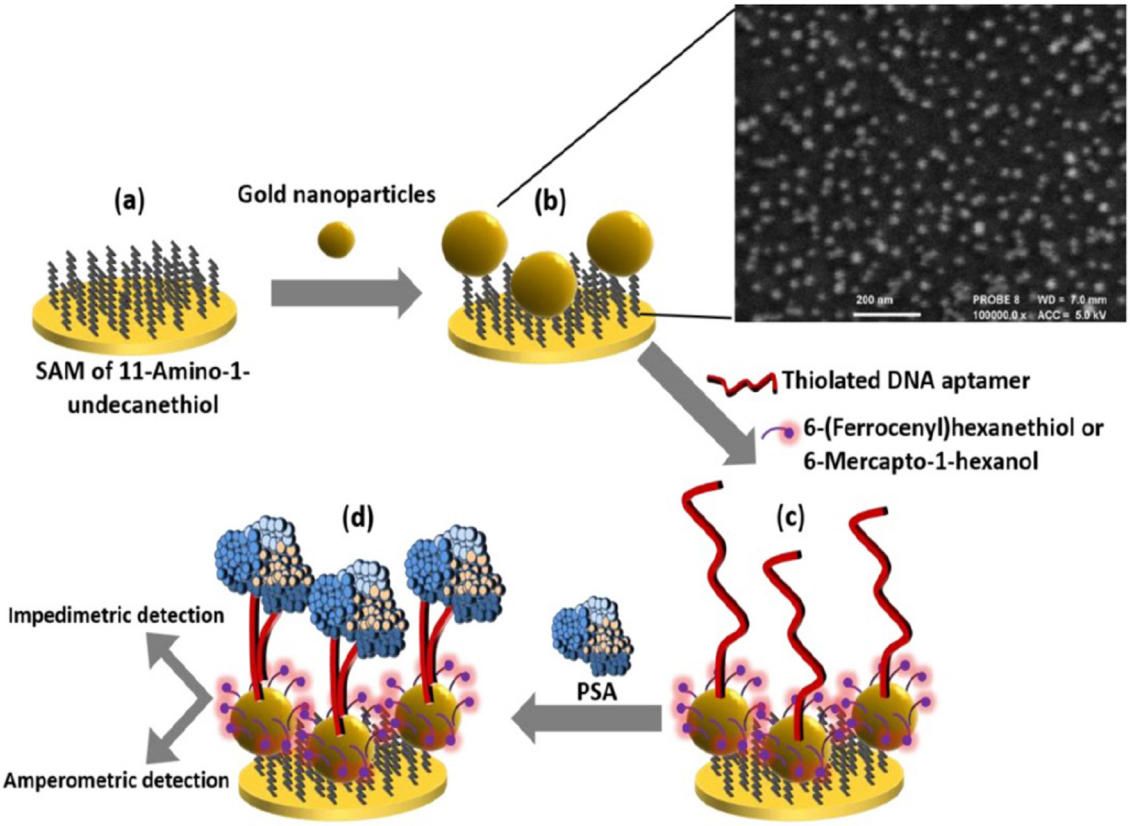

Fig. 1. Schematic representation of a PSA aptasensor fabrication using Au NPs and a 11-amino alkanethiol (Permission No: 4540250617264).

capability, and stability [22,23]. The systematic evolution of the ligands by exponential enrichment (SELEX) process was followed toward the glycosylation site of the glycoprotein as a case of PSA and an important sign for cancer growth [24]. Here, a PSA aptamer was electrochemically used in a sandwich form against PSA [25]. Another sandwich sensing platform was established where a capturing aptamer was immobilized on the surface of an Au screen-printed electrode. Another detecting aptamer was applied that in the presence of PSA, a sandwich structure was formed. This aptasensor had a linear range of PSA detection in serum from 0.66 to 62.5 ng mL^{-1} with a limit of detection (LOD) of 0.66 ng mL^{-1}. Magnetic NPs@gold NPs (Au NPs) were applied in another SERS PSA aptasensor [26]. The used core-shell NPs consisted of a core of magnetic NPs with a size of 500 nm and a gold shell of 30 nm. PSA aptamer was bound on the magnetic NPs and an aptamer-complementary sequence was bound on the Au NPs surface. In the absence of PSA, the aptamer and its complementary sequence provided a double strand. In the presence of PSA and due to the higher affinity of PSA into the aptamer, the complementary sequence was released. This event led to changes in SERS signals and subsequently detection of PSA in a range of 1 to 50 ng mL^{-1} with a LOD of 5 pg mL^{-1}. Exciton-plasmon interaction between CdS quantum dots (QDs) functionalized with mesoporous TiO_2 and Au NPs led to designing a photoelectrochemical PSA aptasensor [27]. Firstly, a fluorine-doped tin the oxide electrode was modified with CdS QDs/TiO_2 nanostructure and subsequently, a thiolated capturing DNA was conjugated on the surface by Cd-S bond. In the next step, a thiolated PSA aptamer was conjugated with Au NPs. In the presence of PSA, the sandwich structure formed between the aptamer, capturing DNA was broken, and the aptamer captured PSA with a good affinity. This aptasensor was able to determine PSA in the range of 1 pg mL^{-1} to 8 ng mL^{-1} with a LOD of 0.52 pg mL^{-1}. A fluorescence PSA aptasensor was designed based on metal-organic frameworks and Au nanoparticles in a core-shell structure [28]. A high-affinity aptamer was bound with Au nanoparticles that quenched the fluorescence of the frameworks. In the absence of PSA, aptamer represented a protective role against the aggregation of Au nanoparticles leading to fluorescence quenching. This mechanism created an aptasensing platform against PSA with a LOD of 0.36 ng mL^{-1}. An innovative PSA detection route was reported in a fluorescent aptasensor using anionic tetraphenylethylene derivative of 1,2-bis[4-(3-sulfonatopropoxyl)-phenyl]-1,2-diphenylethene sodium salt 3 (TPE3), as an aggregation-induced emission agent [29]. Here, positively charged silica nanospheres with an average diameter of 80 nm absorbed the negatively charged PSA aptamer and TPE3, separately. In the presence of PSA, the conformation of aptamer was changed upon binding with PSA. This event led to the destruction of binding between the aptamer and silica nanospheres; TPE3 was aggregated on the surface of the silica nanospheres and the fluorescence signals were changed. The linear range of this aptasensor was 0.5 to 50 ng mL^{-1} and LOD was 0.5 ng mL^{-1}. Colloidal MoS_2 nanosheets were applied in another fluorescent PSA aptasensor [30]. A single-stranded DNA (ssDNA) aptamer was firstly immobilized on the surface of MoS_2 nanosheets (as a high fluorescence-quenching agent), and the aptamer was labeled with a fluorescent agent from 5′ end. In the presence of PSA, the aptamer underwent conformation changes followed by release from the surface of MoS_2 nanosheets. This aptasensor was able to detect PSA in a range of 0.5 to 300 ng mL^{-1} and LOD was 0.2 ng mL^{-1}. A PSA aptasensor was developed based on guanine-rich DNA aptamer-conjugated 6-carboxyfluorescein [31]. Free guanine-rich DNA aptamer-conjugated 6-carboxyfluorescein emitted bright light due to chemiluminescent resonance energy transfer between 6-FAM and high-energy intermediate formed from the reaction of 3,4,5-trimethoxylphenylglyoxal and guanine of guanine-rich DNA aptamer. After PSA binding, it acted as a strong interference in chemiluminescent resonance energy transfer, and light emission turned off. This aptasensor was able to detect PSA in the range of 1.9 to 125 ng mL^{-1} with a LOD of 1 ng mL^{-1}. A modified gold electrode with Au NPs (20 nm) was

used to design a PSA aptasensor [32]. The increased surface of the gold electrode provided a high surface concentration of the aptamer. As shown in Fig. 1, in the first step, the surface of the gold electrode was modified with 11-amino alkanethiol to prepare a high-density monolayer. In the next step, unwanted thiol fragments were removed and mercaptohexanol was immobilized in the remaining uncovered gold sites. Subsequently, the electrode was modified with Au NPs, and aptasensor was prepared after binding thiolated aptamer from 5′ end to Au NPs. Finally, PSA detection was separately followed by electrochemical impedance spectroscopy (EIS) and SWV. This signal-off aptasensor could detect PSA by EIS in a range of 0.01 to 10 ng mL^{-1} and a LOD of 0.01 ng mL^{-1}, and SWV in a range of 1 to 100 ng mL^{-1} and a LOD of 0.1 ng mL^{-1}.

In another research, Ag NPs were synthesized and applied for binding with an amine functionalized PSA aptamer [33]. In this aptasensor, three thiolated DNA aptamers were bound with the surface of the gold electrode, followed by Ag NPs binding into the aptamers. When PSA molecules did not exist, the amine-functionalized aptamer was able to create a double-stranded couple with the other remained free aptamers. In the presence of PSA, amine-functionalized aptamer showed a higher affinity toward PSA molecules for binding against free aptamers. This property led to the detection of PSA in a range of 1 pg mL^{-1} to 160 ng mL^{-1} with a LOD of 0.11 pg mL^{-1}. A screen-printed carbon electrode was used in a PSA aptasensor where Au NPs (15–25 nm) were electrodeposited to enhance the surface area and improve the electron transfer rate [34]. In this biosensor, a mercaptoalkane was bounded with Au NPs, and carboxyl groups of 16-mercaptohexadecanoic acid reacted with the amine group of a PSA aptamer. Then, the aptamer captured the PSA and was detected by EIS in a range of 0 to 10 ng mL^{-1}; also, LOD was reported as 1.95 ng mL^{-1}. In a research, four ssDNA including a thiolated PSA aptamer, a cDNA-primer, a rolling circle amplification (RCA) template, a thiolated probe, and Fe_3O_4 core-gold shell NPs were employed for electrochemical detection of PSA [35]. The thiolated PSA aptamer was immobilized on the NPs surface followed by hybridization with a part of cDNA-primer. The other part of the cDNA-primer was then hybridized with the RCA template. This structure underwent interaction with MB and immobilization on the thiolated probe; the thiolated probe was already immobilized on the Au NPs-covered electrode. In the presence of PSA, less aptamer-cDNA-primer hybridization occurred and less MB interacted. This aptasensor was able to detect PSA in a linear range from 100 fmol L^{-1} to 10 nmol L^{-1}, and the LOD was reported as 22.3 fmol L^{-1}. A summary of the working principle of this aptasensor is presented in Fig. 2.

An aptasensor was designed based on graphene modified electrodes for PSA detection [36]. A carbon surface was modified with graphene to enhance surface concentration of an immobilized amine-aptamer. This was followed by hybridization with a complementary sequence. In the presence of PSA, most of the established double-stranded DNA was broken to bind with PSA. Using the intercalator methylene blue, PSA binding was followed. An electrochemical PSA aptasensor was developed based on RCA and Cu NPs [37]. This aptasensor could detect PSA in a range of 0.05 to 500 fg mL^{-1} and with a LOD of about 0.020 fg mL^{-1}. Mesoporous silica provided an enhanced surface area of a gold electrode for capturing PSA in another study [38]. The transducer surface was prepared by aptamer binding with 3-glycidyloxypropyl trimethoxysilane through amine groups. Fig. 3 shows a schematic presentation of this PSA aptasensor.

In the presence of PSA, aptamer captured PSA molecules with a high affinity, and the redox marker could not attain the transducer surface. In our research group, a PSA aptasensor based on a hairbrush-like gold nanostructure was developed [39]. The nanostructure was electrodeposited in the presence of cadaverine as a shape and size controlling agent. Covering a gold electrode surface with the hairbrush-like gold nanostructure led to increment in the real surface area by 1.6 times, leading to an enhanced aptasensing sensitivity. We also developed a PSA aptasensor based on a PSA aptamer immobilized on the surface of gold nanospears prepared by electrodeposition in the presence of arginine in the synthesis solution [40]. Binding of PSA changed the conformation of aptamer strands leading to changes in the rate of electron transfer of MB, as the redox marker. This aptasensor was able to detect PSA in a range of 0.125 to 200 ng mL^{-1} and a LOD of 50 pg mL^{-1}. An ECL PSA aptasensor was introduced [41]. To fabricate this aptasensor, we firstly synthesized a signal nanocomposite comprising graphene oxide (GO), gold nanorods (NRs), streptavidin (STP) and a biotin-labeled DNA. To synthesis the nanocomposite, Au NRs were deposited on GO based on the electrostatic interaction of GO (negatively charged) and cetyltrimethylammonium bromide (CTAB)-capped Au NRs (positively charged). STP was then conjugated with GO@Au NRs by mixing. After that, a biotin-labeled ssDNA that was complementary with the head of a PSA aptamer was immobilized on the previously prepared mixture. In a parallel manner, a thiolated ssDNA sequence that was complementary with the tails of the PSA aptamer was hybridized with the aptamer followed by immobilization on the surface of a gold-covered carbon electrode. The signal nanocomposite was finally hybridized with the modified electrode surface. In the presence of PSA, it's binding with the aptamer led to the release of the signal nanocomposite that catalyzed the production of hydrogen peroxide; hydrogen peroxide thereafter converted (electrochemically formed) the luminal radical to 3-aminophthalate by Au NRs catalytic effect and produced light. This ECL PSA aptasensor quantified PSA in a range of 0.5 pg mL^{-1} to 5 ng mL^{-1} and LOD was 0.17 pg mL^{-1}. A quinone-based conducting polymer was used as a transducer to immobilize an amine-functionalized PSA aptamer, and PSA detection with a LOD of 0.25 ng mL^{-1} [42]. Amine-functionalized PSA aptamer was also immobilized on carboxylic acid-functionalized carbon nanotubes that adhered to a glassy carbon electrode by chitosan by themselves [43]. Multiple layers of electropolymerized polydopamine, as a scaffold, were prepared by molecular imprinting for fixing the aptamer strands [44]. This scaffold provided some specified binding locations for selective attachment of PSA, and other proteins could not bind into these sites. Electrochemical measurements were then employed for PSA detection. GO and carboxylated multiwall carbon nanotubes (MWCNTs) were dropped on the surface of the glassy carbon electrode, GO was electrochemically reduced, and finally, Au NPs were electrodeposited. This substrate was used to immobilize a thiolated aptamer for PSA sensing. This aptasensor could detect PSA (0.005–100 ng mL^{-1}) and the reported LOD was 1 pg mL^{-1} [45]. Au NPs-mesoporous carbon modified with STP was also applied to immobilize a biotinylated PSA aptamer followed by electrochemical detection [46].

The first PSA electrochemical aptasensor based on memristive effect was developed in 2016 [47]. Hysteretic properties of memristive silicon nanowires functionalized with biotin-DNA aptamers provided a LOD of 23 amol L^{-1}. Upon PSA binding with the aptamers, extra charges surrounded the device, created an all-around bio-gate effect and induced a voltage gap in the current-voltage characteristics. Two aptamers were used as a sandwich format in a PSA immunosensors, and an immunocomplex was established among the antibody, PSA and the aptamers [48]. An amine-functionalized aptamer was applied to fabricate a PSA immunosensor [49]. The details about these immunoassays will be discussed in Section 4.

Analytical aspects and features of major PSA aptasensors are collected and compared in Table 1. The functional groups of aptamers included thiol, biotin, and amine. In most of these PSA aptasensors, the usage of nanostructures led to the enhancement of sensitivity.

3. PSA peptisensors

Peptides are naturally or artificially synthesized through the polymerization of amino acids by desired peptide bonds between the carboxyl groups [57]. Fast and low-cost production, easy functionalization, high stability and the same genus against most of the disease

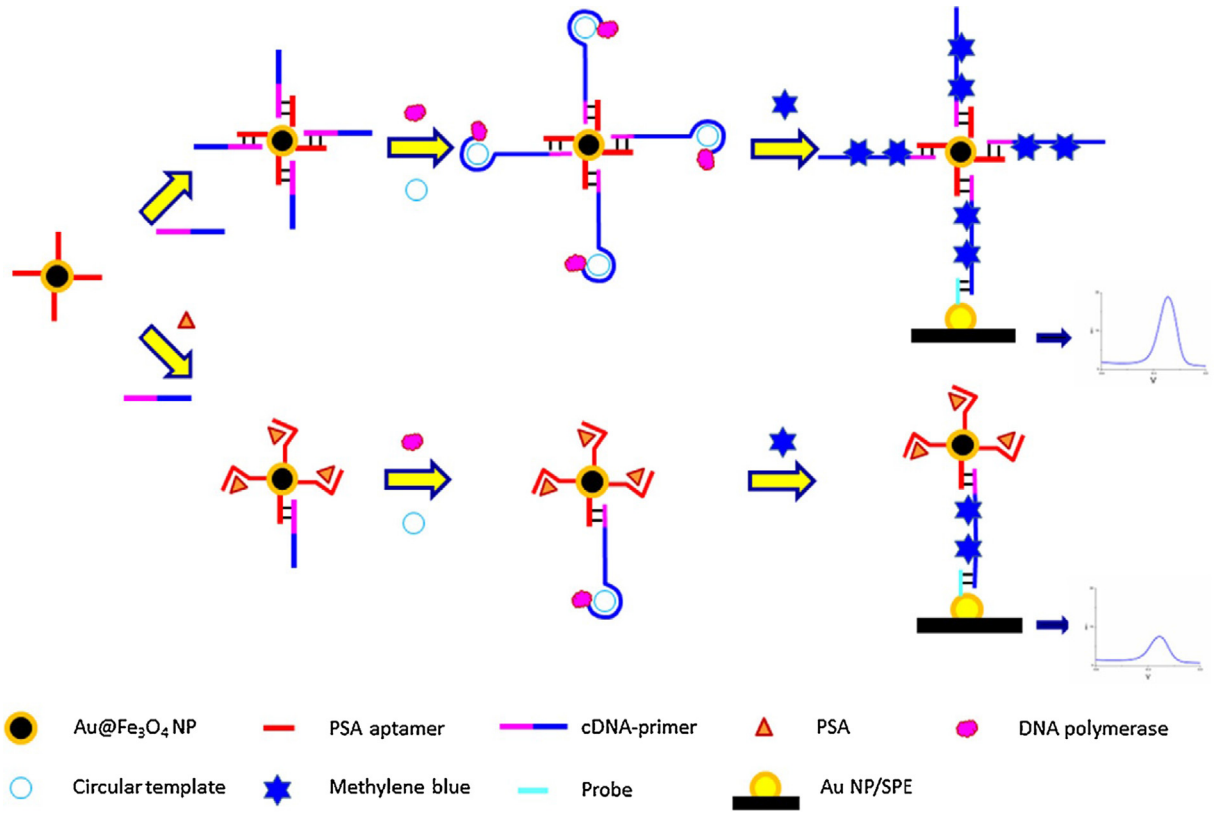

Fig. 2. Schematic representation of a PSA aptasensor based on four strands of a thiolated PSA aptamer, a cDNA-primer, a RCA template and a thiolated probe, and gold shell-Fe_3O_4 core NPs were employed for electrochemical detection of PSA (Permission No: 4643450320566).

biomarkers are some of the advantages of peptide sequences application in biosensors fabrication [58,59]. We have introduced the term "peptisensor" for peptide-based biosensors for the first time [60]. In all of the peptide sequences hitherto employed to design PSA peptisensors, a sequence of KLQ was present. This is due to the breakdown of the peptide in this region.

So far, peptides have been used in the structure of some PSA biosensors. A fluorescence PSA peptisensor was designed based on site-specific enzymatic-cleavage-reaction [61]. In this peptisensor, Au NPs (60 nm) were conjugated with a specific peptide already bound with fluorescein isothiocyanate (FITC). The peptide included three parts: six cysteine residues that were conjugated the peptide into Au NP, an α-isobutyric acid residue that maintained the rigidity of the peptide, and a PSA cleavage sequence. In the presence of PSA, an enzymatic-cleavage-reaction occurred, the peptide sequence broke, and the bound fluorescence was released and emitted light. Another fluorescent PSA peptisensor was designed using a FITC-labeled peptide and 1-nm thick GO, as a nanoquencher [62]. The working principle of this peptisensor was similar to the previous reference.

As for electrochemical peptisensing of PSA, a thin layer of Au NPs was firstly electrodeposited followed by modification with dithiobis (succinimidyl propionate) [63]. A PSA specific peptide was immobilized on the modified surface from one side, and Au NPs were bound into the other side of the peptide. These atop Au NPs were then integrated with (positively charged) CTAB to make Au NPs to carry a positive charge. Adsorption of the negatively charged $[Fe(CN)6]^{3-/4-}$ probe led to its electron transfer with the underlying surface. Upon PSA binding, a serine protease specifically hydrolyzed and cleaved the peptide, and the positively charged Au NPs were released from the electrode surface; this later led to high electro-transfer resistance. This peptisensor was able to quantitatively detect PSA in a range of 0.2 pg mL^{-1} to 45 ng mL^{-1} and LOD was 0.06 pg mL^{-1}. A schematic presentation of this PSA peptisensor is shown in Fig. 4.

In other researches [64,65], PSA led to cleavage of a specific peptide

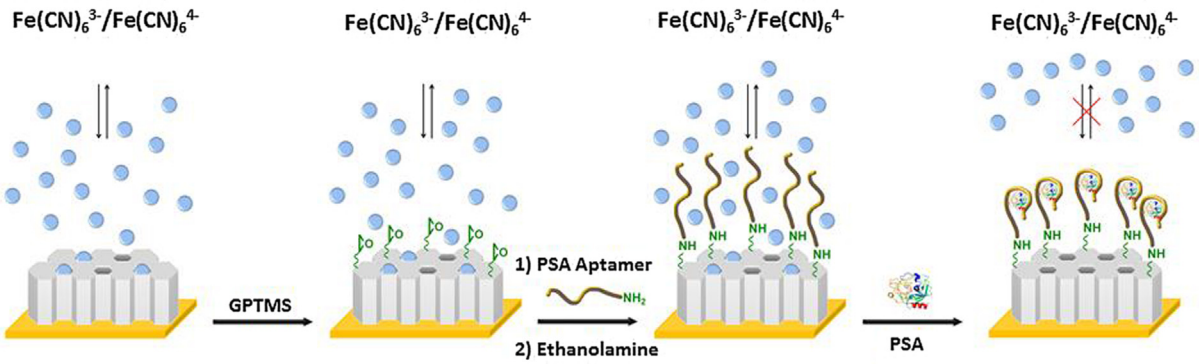

Fig. 3. Fabrication and working principals of a PSA aptasensor based on mesoporous silica and an amine-functionalized aptamer (Permission No: 4541811332818).

Table 1
A comparison of various PSA aptasensors.

Aptamer sequence (5′→3′)	Nanostructure	Detection technique	Detection range	LOD	Sensitivity	Specificity	Sample/ number	Ref.
SH-T_{10}ATTAAAGCTCGCCATCAAATAGCTGC-3′	Au@Ag NPs	SERS	0.01–5 fmol L^{-1}	4.8 amol L^{-1}	–	–	Serum/6	[50]
NH_2-TTTTTTTTTTATTAAAGCTCGCCATCAAATAGCTGC	Magnetic NPs@Au NPs	SERS	1–50 ng mL^{-1}	5 pg mL^{-1}	–	–	Serum/3	[26]
CGATGGCATATTAAAGCTCGCCATCAAATAGCGTGGCCTGG	Au upconversion NPs	SERS	0–1 amol L^{-1}	0.032 amol L^{-1}	–	–	Serum/6	[51]
SH-$(CH_2)_6$-ATTAAAGCTCGCCATCAAATAGC-3′	Au NPs	RLS	0.13–110 ng mL^{-1}	0.032 ng mL^{-1}			Serum/15	[52]
NH_2–$(CH_2)_6$-ATTAAAGCTCGCCATCAAATAGC-biotin	Au NPs/GO	DPV	0.1 pg mL^{-1}-90 ng mL^{-1}	10 fg mL^{-1}	–	–	Serum/5	[48]
(Thiolated)[1] ATTAAAGCTCGCCATCAAATAGC	Au NPs/GO	DPV	0.05 pg mL^{-1}-200 ng mL^{-1}	10 pg mL^{-1}	–	–	Serum/21	[53]
NH_2–$(CH_2)_6$-TTTTTAATTAAAGCTCGCCATCAAATAGCTTT	Mesoporous silica	DPV	1–300 ng mL^{-1}	280 pg mL^{-1}	1.03 μA mL ng^{-1} cm^{-2}	–	Serum/5	[38]
SH-$(CH_2)_6$-TTTTTAATTAAAGCTCGCCATCAAATAGCTTT-MB	Hairbrush-like Au nanostructure	DPV	0.125–128 ng mL^{-1}	50 pg mL^{-1}	–	–	Serum/10	[39]
biotin-TTTTTAATTAAAGCTCGCCATCAAATAGCTTT	Au NPs@GMCs	DPV	0.25–200 ng mL^{-1}	0.25 ng mL^{-1}	–	–	–	[46]
SH-$(CH_2)_6$-TTTTTAATTAAAGCTCGCCATCAAATAGCTTT	Au nanospears	DPV	0.125–200 ng mL^{-1}	50 pg mL^{-1}	–	–	Serum/10	[40]
TTTTTAATTAAAGCTCGCCATCAAATAGCTTTCCCCC	CNTs-chitosan	DPV	0.85–12.5 ng mL^{-1}	0.75 ng mL^{-1}	0.0026 mA ng^{-1} mL	–	Serum/2	[43]
SH-$(CH_2)_6$-ATTAAAGCTCGCCATCAAATAGC	Au NPs	RLS	0.13–110 ng mL^{-1}	0.032 ng mL^{-1}	–	–	Serum/15	[52]
NH_2–$(CH_2)_6$-ATTAAAGCTCGCCATCAAATAGCTGCTAA	Ag NPs	LSV	1 pg mL^{-1}-160 ng mL^{-1}	0.11 pg mL^{-1}	–	–	Serum/6	[33]
SH-TTAATTAAAGCTCGCCATCAAATAGC	Au NPs/graphene nanosheet, CdS QDs/TiO_2	Photoelectrochemical sensing	1 pg mL^{-1}-8 ng mL^{-1}	0.52 pg mL^{-1}	–	–	Serum/8	[27]
TTATTAAAGCTCGCCATCAAATAGC	SiO_2 NPs	Fluorescent	0.5–50 ng mL^{-1}	0.5 ng mL^{-1}	–	–	Serum/5	[29]
FAM-TTATTAAAGCTCGCCATCAAATAGC	MoS_2 nanosheet	Fluorescent	0.5–300 ng mL^{-1}	0.2 ng mL^{-1}	–	–	Serum/8	[30]
TTAATTAAAGCTCGCCATCAAATAGC	GO@Au NRs	ECL	0.5 pg mL^{-1}-5 ng mL^{-1}	0.17 pg mL^{-1}	–	–	Serum/8	[41]
1: 6-FAM-TTTTTAATTAAAGCTCGCCATCAAATAGCTTT2: TTTTTAATTAAAGCTCGCCATCAAATAGCTGGGGG-6-FAM	Fe_3O_4 MWCNT	Chemiluminescent	1.9–125 ng mL^{-1}	1 ng mL^{-1}	–	–	–	[31]
Biotin-TTTTTAATTAAAGCTCGCCATCAAATAGCTTT	Si nanowires	Electrical memristive sensing	33 amol L^{-1}-330 fmol L^{-1}	23 amol L^{-1}	–	–	–	[47]
SH-$(CH_2)_6$-TTTTTAATTAAAGCTCGCCATCAAATAGCTTT	–	EIS	100 pg mL^{-1}-100 ng mL^{-1}	1 pg mL^{-1}	–	–	–	[44]
SH-$(CH_2)_6$-TTTTTAATTAAAGCTCGCCATCAAATAGCTTT	GO/MWCNT/Au NPs	EIS	0.005–100 ng mL^{-1}	1 pg mL^{-1}	–	–	Serum/4	[45]
SH-$(CH_2)_6$-TTTTTAATTAAAGCTCGCCATCAAATAGCTTT	–	EIS	1–10 ng mL^{-1}	1 ng mL^{-1}	–	–	–	[54]
NH_2–$(CH_2)_6$-TTTTTAATTAAAGCTCGCCATCAAATAGCTTT	Au NPs	EIS	0–10 ng mL^{-1}	1.95 ng mL^{-1}	–	–	–	[34]
SH-$(CH_2)_6$-TTTTTAATTAAAGCTCGCCATCAAATAGCTTT	Au NPs	EIS/SWV	10 pg mL^{-1}-10 ng mL^{-1}	10 pg mL^{-1}	–	–	Serum/5	[32]
SH-$(CH_2)_6$-AATTAAAGCTCGCCATCAAATAGCTTT	Fe_3O_4/Au@Fe_3O_4 NPs	CV/EIS/SWV	100 fmol L^{-1}-10 nmol L^{-1}	22.3 fmol L^{-1}	–	–	–	[35]
SH-TTTTTAATTAAAGCTCGCCATCAAATAGCTGGGGG-MB	–	SWV	0.08–100 ng mL^{-1}	0.08 ng mL^{-1}	–	–	–	[55]
NH_2–$(CH_2)_6$-TTTTTAATTAAAGCTCGCCATCAAATAGCTTT	–	SWV	1 ng mL^{-1}-10 μg mL^{-1}	0.25–200 ng mL^{-1}	–	–	–	[42]
SH-TTATTATTAAATTAAAGCTCGCCATCAAATAGCTTT	Cu NPs	DPSV	0.05–500 fg mL^{-1}	0.020 fg mL^{-1}	–	–	Serum/12	[37]
SH-$(CH_2)_6$-ATTAAAGCTCGCCATCAAATAGC	–	Microfluidic love-wave sensor	10 ng mL^{-1}-1 μg mL^{-1}	10 ng mL^{-1}	–	–	–	[56]

1. It is not clear that what end of the sequence was thiolated.
Abbreviations:
LSV: Linear sweep voltammetry.
EIS: Electrochemical impedance spectroscopy.
DPSV: Differential pulse stripping voltammetry.
CV: Cyclic voltammetry.
RLS: Resonance light scattering.
GMCs: Graphitized mesoporous carbon NPs.
CNT: Carbon nanotubes.
SWV: Square wave voltammetry.

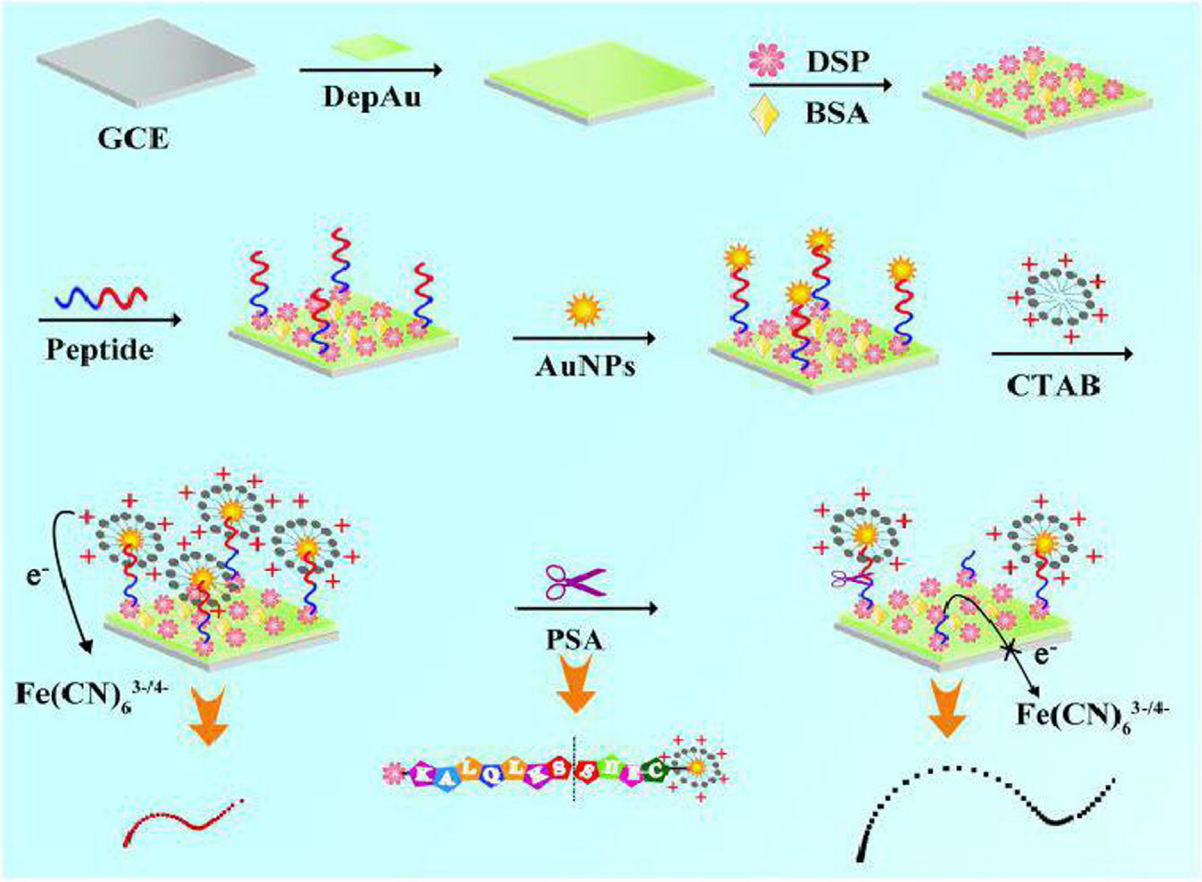

Fig. 4. A PSA peptisensor fabrication steps by Au NPs, CTAB and a 11-mer peptide sequence (Permission were obtained from Royal Society of Chemistry).

sequence, and produced current due to redox transition of a ferrocene (Fc) label [65] or deposited Ag NPs [64] with nearly the same LODs. In another electrochemical PSA peptisensor, 4-azidoaniline covalently immobilized an ethynyl-functionalized peptide probe by click coupling, and 2-[(4-aminophenyl)sulfanyl]-8-hydroxy-1,4-naphthoquinone played the role of an electrochemical transducer of the peptide-protein recognition [66]. The peptide with a sequence of HSSKLQL was cleaved in the presence of PSA, and the output signal was changed. This biosensor could determine PSA in a linear range of 1×10^{-12} to 1×10^{-6} mol L^{-1}, using CV and SWV techniques. A modified glassy carbon electrode with chitosan-lead ferrocyanide-(poly (diallyldimethylammonium chloride)-GO), as a porous and conductive substrate, was prepared [67]. To improve the sensitivity, they bound bovine serum albumin (BSA) molecules on the peptide, and then various concentrations of PSA were determined via SWV and EIS. The presence of PSA led to the cleavage of the immobilized peptide and increment in the electrochemical current.

In an ECL-based PSA peptisensor, tris (2,2′-ripyridine) dichlororuthenium (II) (Ru(bpy)3^{2+}, as an ECL emitting species), was absorbed on a film of Au NPs and Nafion followed by immobilization of a ferrocene carboxylic acid (as an ECL signal quencher) labeled-peptide sequence [68]. All of these components were placed on a glassy carbon electrode surface. When PSA was present, it specifically cleaved the peptide sequence, left the ECL signal quencher and resulted in an increase in the ECL intensity. This biosensor represented a LOD of 8×10^{-13} g mL^{-1}. In another PSA peptisensor based on ECL, the peptide employed in the aforementioned study was labeled with ruthenium bis(2,2′-bipyridine) (2,2′-bipyridine-4,4′-dicarboxylic acid)-N-hydroxysuccinimide ester and immobilized on a gold electrode surface [69]. Similar to the previous study, PSA specifically cleaved the peptide, and the ECL signal decreased. However, the LOD value was larger and equal to 3.8×10^{-11} g mL^{-1}.

In a study, the wells of a 96-well plate were modified with Au NPs to provide a surface for immobilization of biotin functionalized peptide [70]. Then, magnetic beads with coats of both STP and invertase were bounded with the peptide. The presence of PSA led to peptide cleavage and release of the beads that then catalyzed the conversion of fructose and glucose. The concentration of glucose was monitored as the PSA concentration and determined by a glucometer.

According to the results summarized from all designed peptide-based PSA biosensors, it should be noted that all of them were based on the cleavage of a peptide used as biorecognition element in the presence of PSA, and so far, it has not presented any PSA peptisensor based on capturing the PSA as a biorecognition element. Another point is that most of the reviewed PSA peptisensors evaluated the serums as the real samples and only one research used spiked PSA in the urine samples to evaluate the performance of the related biosensor in real conditions. Details about all the designed PSA peptisensor are presented in Table 2.

4. PSA immunosensors

Although antibodies have similar constructional features, they show a wide variety and significant differences in their binding regions against antigens [71,72]. Because of the high specificity and affinity, antibodies are considered as ideal biological diagnostic elements. An electrochemical PSA immunosensor was designed based on molecularly imprinted polymer (MIP) and a nanocomposite containing Fe_3O_4 nanoparticles, graphene oxide, multi-walled carbon nanotube and a PSA antibody [73]. Impedimetric signals of this immunosensor led to PSA determination with a LOD of 5.4 pg mL^{-1}. Pd@Au@Pt nanocomposites were electrodeposited on COOH-terminated reduced GO followed by immobilization of an anti-PSA on the graphene surface through 1-ethyl-

Table 2
Main details of PSA peptisensors.

Peptide sequence	Nanostructure	Detection technique	Detection range	LOD	Real sample type/ number	Ref.
N'-CCCCCCGLAibAAGGHSSLKQGK-FITC-C'	Au NPs	Fluorescent	10 pmol L^{-1}-100 nmol L^{-1}	10 pmol L^{-1}	–	[61]
FITC-EHSSKLQLAK-NH_2	GO	Fluorescent	0.5–3 nmol L^{-1}	0.3 nmol L^{-1}	Urine/3	[62]
CEHSSKLQLAK-NH_2	Au NPs	CV/EIS	0.2 pg mL^{-1}-45 ng mL^{-1}	0.06 pg mL^{-1}	Serum/4	[63]
HSSKLQ	Fe_3O_4@Au nanocomposites	DPV	0.001–30 ng mL^{-1}	0.78 pg mL^{-1}	Serum/4	[65]
CEHSSKLQLAK-NH_2	MWCNTs	LSV	0.001–30 ng mL^{-1}	0.7 pg mL^{-1}	Serum/5	[64]
HSSKLQL	–	CV/SWV	1×10^{-12}-1×10^{-6} mol L^{-1}	–	–	[66]
CEHSSKLQLAK-NH_2	–	SWV/EIS	1 fg mL^{-1}-100 ng mL^{-1}	1 fg mL^{-1}	Serum/15	[67]
CHSSKLQK	Au NPs	ECL	5 pg mL^{-1}-5 ng mL^{-1}	0.8 pg mL^{-1}	Serum/8	[68]
CHSSKLQK	–	ECL	0.1–8 ng mL^{-1}	38 pg mL^{-1}	Serum/3	[69]
Biotin-EHSSKLQKC	Au NPs	A glucometer	80 pg mL^{-1}-7 ng mL^{-1}	30 pg mL^{-1}	Serum/5	[70]

3-(3-(dimethylaminopropyl) carbodiimide/N-hydroxysuccinimide (EDC/NHS) system and electrochemical detection [74]. Graphene itself was drop-cast on an Au/Ti (150/30 nm) coated Si/SiO_2 substrate. An intrinsic reduction peak of the trimetallic nanocomposites (appearing in the cyclic voltammograms recorded in phosphate buffer solution 0.1 mol L^{-1}, pH 7.4) that had the highest current, compared to the bimetallic or monometallic NPs and was affected by PSA binding into the immobilized anti-PSA, was employed for quantitation of PSA. In the trimetallic system, geometrical structure (i.e. reduced Pt-Pt bond distance) and electronic (i.e. an increased Pt d-electron vacancies) alterations would be dominated. EIS technique was used in order to determine PSA by another immunosensor [75]. Here, the working area of a gold screen-printed electrode was firstly covered with cystamine through Au-S bond. Then, Fc and polyamidoamine dendrimer (PAMAM) were prepared and attached on the surface by glutaraldehyde (as a cross-linker). Subsequently, a PSA antibody was covalently immobilized on the surface that could capture PSA molecules. To create a sandwich PSA immunosensor, another PSA antibody that was tagged with horseradish peroxidase was applied. The presence of PSA led to the capture of more PSA and also the creation of more sandwich forms between the two antibodies. The schematic presentation of this PSA immunosensor is shown in Fig. 5. Electrochemical immunosensing of PSA was also followed using multi-walled carbon nanotube and Au NPs [76]. This biosensor transducer comprised functionalized multiwall carbon nanotubes decorated with Au NPs and its biorecognition element was a mouse monoclonal PSA antibody. In another electrochemical PSA immunosensor, a modified glassy carbon electrode with GO and chitosan film was used as a transducer [48]. Sandwich immunoreaction among the PSA, PSA antibody and an aptamer was followed. PAMAM encapsulated Au NPs were applied as a covalent electrochemical attachment label to increase sensitivity. This immunosensor could detect PSA in two separate ranges and LOD based on detection method; a detection range of 0.1 pg mL^{-1} to 90 ng mL^{-1} and a LOD of 10 fg mL^{-1} were attained by DPV, and up to to35 ng mL^{-1} with a LOD of 5 pg mL^{-1} were obtained by EIS.

An ECL PSA immunosensor was introduced based on CdWS nanocrystals integrated onto Ag^+@UIO-66-NH_2 to create an Ag^+@UIO-66-NH_2@CdWS ECL nanoprobe [77]. In this immunosensor, a glassy carbon electrode was modified with reduced GO and Au NPs, leading to an enhanced surface area and also improved sensitivity. Then, a specified PSA antibody was immobilized on the surface of the modified electrode. To accelerate the ECL signal in the presence of PSA, another antibody was conjugated with Ag^+@UIO-66-NH_2@CdWS nanostructure that could capture the PSA from the other side to form a sandwich structure. The schematic details of this immunosensor are presented in Fig. 6. Another ECL PSA immunosensor was presented based on luminol functionalized platinum NPs loaded on the graphene sheets [78]. Luminol played the roles of both a reducing agent to synthesize Pt NPs on the surface of graphene sheets and a luminescence reagent. Pt NPs supplied active sites for the immobilization of PSA antibodies and enhanced the ECL signals of luminol by catalyzing the luminol-H_2O_2 reaction. LOD for this immunosensor was 0.3 pg mL^{-1}. In another research, Au NPs functionalized Fe_2O_3 nanodendrites were employed to immobilize a PSA antibody. Separately, Pd NPs functionalized graphene aerogel (FGA-Pd) supported Fe_3O_4 as a 3D carrier, and $Ru(bpy)_3^{2+}$ combined with FGA-Pd as an ECL emitter was assembled to label a secondary antibody, which generated strong ECL signals. Tripropylamine was also employed to react with $Ru(bpy)_3^{2+}$ and generate ECL signals [79]. Nanomagnetic beads were applied in a florescent PSA immunosensor based on DNAzyme [80]. In this immunosensor, a gold electrode was covered with activated carboxyl groups followed by immobilization of an amine-functionalized PSA antibody. After PSA capturing by this antibody, a separately synthesized probe comprised magnetic beads-loaded a DNAzyme and another antibody was bound to form a sandwich structure. A hairpin substrate probe was separately designed with a fluorophore and a quencher at each end. In the presence of Zn^{2+} as a cofactor, DNAzyme cleaved the hairpin substrate probe which was released into the solution and fluorescence emission. In another research, a sandwich immunoassay structure with fluorescence detection was introduced [81]. A PSA capturing antibody was immobilized on a reaction plate modified with NHS esters. Another antibody was labeled with Alexa Fluor 647 and provided a sandwich formation in the presence of PSA. In another detection method, at the first step, a protein was immobilized on the surface of the reaction plate modified with NHS esters and then the capture antibody was immobilized on the protein; the other steps were similar to the other mentioned previous method [81]. In a chemiluminescence PSA immunosensor, PSA antibodies were firstly immobilized on a nitrocellulose membrane and similar to other mentioned sandwich immunoassay methods for the detection of this biomarker, a capture, and a detection antibody were applied [82]. In the presence of PSA, specified capturing and detecting of this tumor marker was evaluated through chemiluminescence by a charge-coupled device. This immunosensor could determine PSA in the range of 0.02 to 125 ng mL^{-1} and the LOD was about 0.007 ng mL^{-1}.

In a sandwich immunosensing route for determination of PSA, phosphorescent dihydrolipoic acid capped Mn-doped ZnS QDs were applied as a label [83]. Herein, microplate wells were modified with rabbit PSA capturing antibody, and then, unwanted reactive sites were blocked by BSA. To produce the sandwich form, a PSA detection antibody was matched with a capture antibody in the presence of PSA. Finally, the bioconjugated nanostructure with antibody was added into the microplates. This phosphorescent immunosensor was able to detect PSA in the range of 0.05 to 240 ng mL^{-1}, while the LOD was 17 pg mL^{-1}.

In a photoelectrochemical PSA immunosensor, Au NPs decorated dopamine-melanin nanospheres (Au NPs-Dpa-melanin CNSs) were applied as a signal quencher based on CdSe-sensitized TiO_2 as a photoelectrochemical matrix [84]. Dpa-melanin CNSs were conjugated with Au NPs, PSA and BSA. In the absence of PSA, PSA-Au NPs-Dpa-melanin

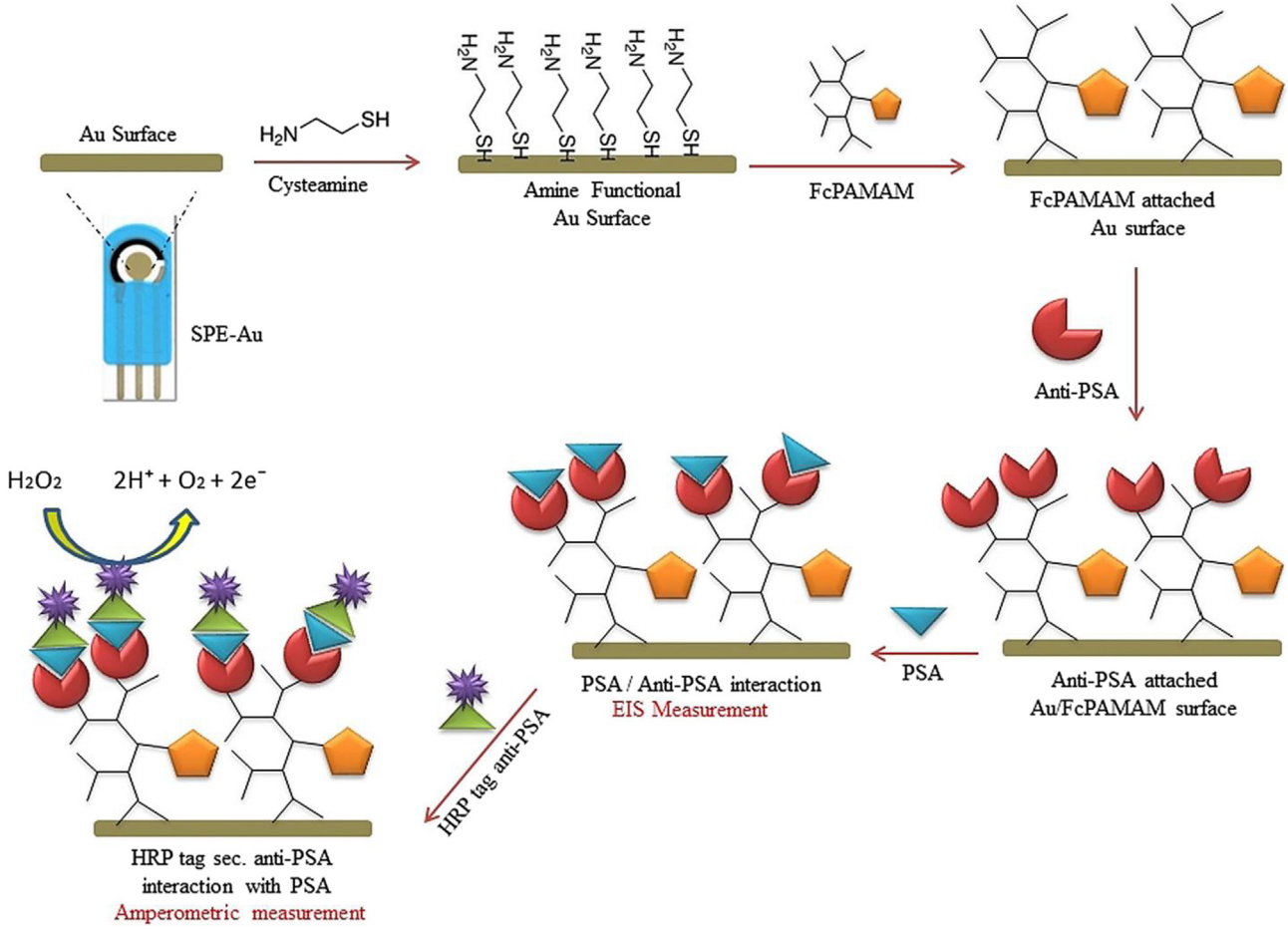

Fig. 5. Design of a PSA immunosensor using Fc and PAMAM (Permission No: 4554381130432).

CNSs could bind with the antibody. However, in the presence of PSA, due to the high affinity of the antibody against PSA, the amount of bound PSA-Au NPs-Dpa-melanin CNSs on the electrode was significantly reduced. This behavior led to the production of different output signals. In another photoelectrochemical PSA immunosensor, a modified surface of indium tin oxide by SnS_2@mesoporous graphite-like carbon nitride (SnS_2@mpg-C_3N_4) nanocomposite was applied [85]. The nanocomposite generated transcendent photocurrents under visible-light irradiation, compared to SnS_2 or mpg-C_3N_4 alone, due to the low recombination rate of photoexcited electron-hole pairs. A PSA antibody was immobilized on the nanocomposite surface, and PSA was detected in a manner that decrement in photocurrent resulted from the increased steric hindrance of the immunocomplex.

Triangular-shape Au NPs was applied in a PSA colorimetric sandwich immunosensor [86]. A capture antibody (Ab1)-conjugated Au NPs bounded PSA in one hand, and formed a sandwich immunoassay platform with another antibody (Ab2)-conjugated Fe_3O_4 NPs. This platform was separated by the magnetic tag, and unbounded Ab1-conjugated Au NPs was determined. This immunoassay platform could detect PSA in a range of 0.01 to 20 ng mL^{-1} with a LOD of 0.009 ng mL^{-1}. A similar approach was applied in another research using near-infrared absorbing Cu_xS nanocrystals in a PSA photothermal immune-imaging assay [87]. A sandwich assembly was prepared that upon PSA capturing, an amplified photothermal signal was generated and analyzed by mobile phone-based digital image processing. This visual immunosensor could detect PSA in the range of 1 to 200 ng mL^{-1}, and LOD was 0.2 ng mL^{-1}. A multicolor and photothermal dual-mode immunosensor was fabricated by immobilization of a platform into 96-well plates [88]. The wells were coated by streptavidin followed by immobilization of a biotinylated PSA aptamer. Separately, a GO/Fe_3O_4/prussian blue nanostructure was synthesized and modified with a (aminated) ssDNA sequence, and served as a signal probe. Without PSA, the signal probe was captured upon hybridization of ssDNA and PSA aptamer. With PSA, this double-stranded structure was broken, and the signal probe was released. The released signal probe was quantified either by temperature measurement upon near-infrared laser irradiation of the prussian blue NPs or naked eye upon mixing with potassium ferricyanide. GO was an enrichment carrier for Fe_3O_4 NPs as well as an enhanced accumulator for prussian blue NPs resulting in signal amplification. This immunosensor could detect PSA in a range of 1 to 128 ng mL^{-1}, and LOD was 0.31 ng mL^{-1}.

A SERS sandwich immunosensing platform for the determination of PSA was introduced based on two separate antibodies [89]. Firstly, the capture antibody was immobilized on a glass substrate. Then, PSA was captured when it existed. The other antibody was conjugated with SERS dots that included silica shell (30 nm), silver NPs (10 nm), silica core (170 nm), and a Raman label. The presence of PSA led to the establishment of a sandwich form between the two antibodies and resulted in a Raman shift. Another SERS-based PSA immunosensor was introduced based on antibody-conjugated SERS nanotags [90]. Here, two types of Raman reporter molecules including malachite green isothiocyanate (MGITC) and X-rhodamine-5-(and-6)-isothiocyanate (XRITC) were used. These molecules were separately immobilized on the surface of Au NPs. At the next step, SH-PEG-COOH was applied to provide conjugated antibody and subsequently this form of antibody was immobilized on the surface of Au NPs via EDC/NHS coupling. The third antibody was immobilized on the surface of carboxylic acid-functionalized magnetic beads by EDC/NHS. It should be noted that, as a

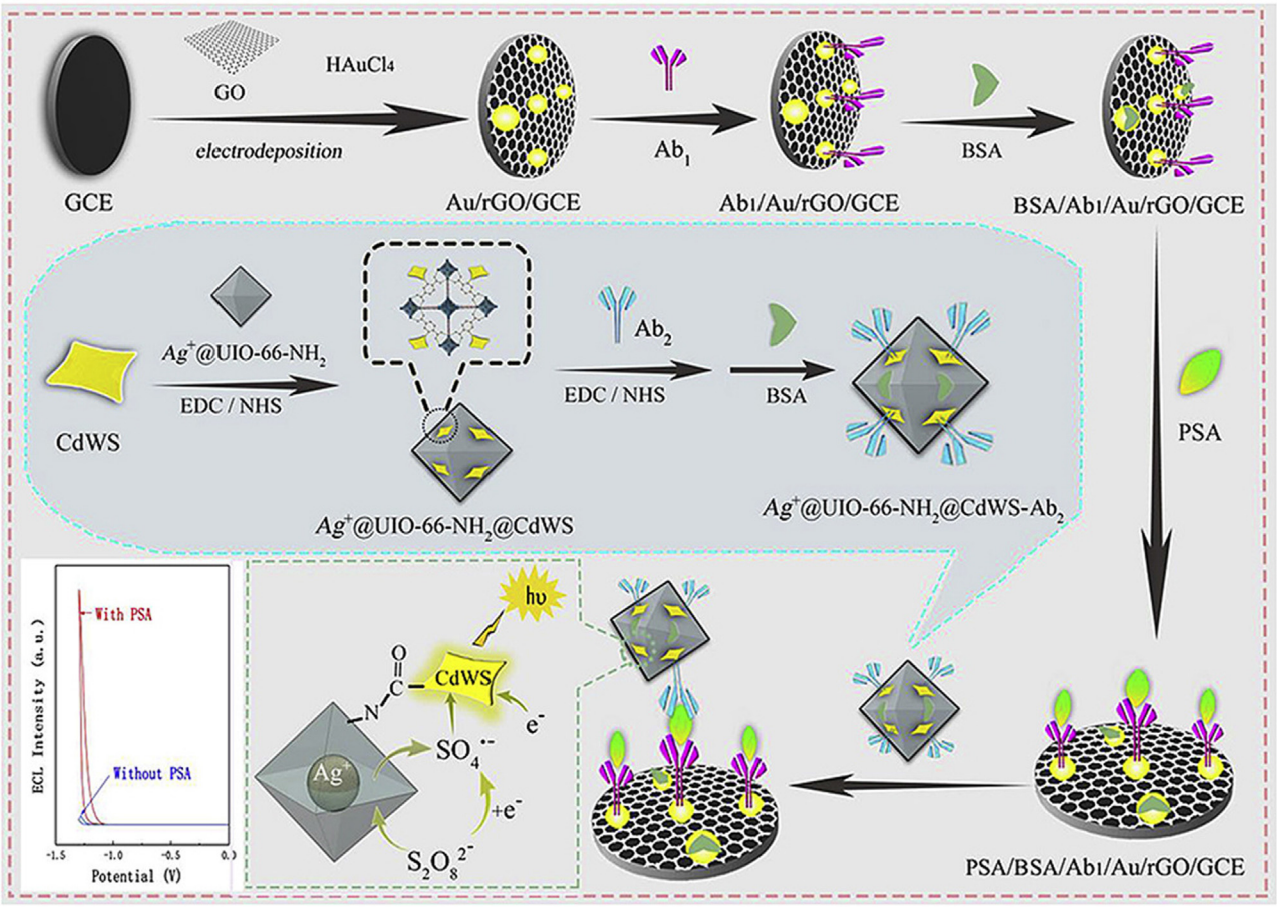

Fig. 6. Schematic details about an ECL PSA immunosensor based on a Ag^{+}@UIO-66-NH_2@CdWS nanostructure (Permission No: 4554380299543).

Raman reporter, the surface that employed MGITC was applied for the determination of free PSA, the surface with XRITC was used for the determination of complexed PSA, and the surface of carboxylic acid-functionalized magnetic beads was applied for the determination of total PSA. This immunosensor was able to detect PSA in the range of 4 to 10 ng mL^{-1} and a LOD was reported as 0.012 ng mL^{-1}. The figure of merits of PSA immunosensors is summarized in Table 3.

5. Other PSA biosensors

In addition to the previous discussed PSA biosensors, those which were based on aptamer, peptide or antibody, several PSA biosensors have been introduced so far that employed other materials as biorecognition elements. Our research team designed an electrochemical biomimetic PSA biosensor based on a molecularly imprinted polymer [169]. In this biosensor, a thin film of polypyrrole was electropolymerized as an artificial antibody. In this study, the transducer was a gold screen-printed electrode that is not reusable and many electrodes are needed for routine analysis. On the other side, PSA is preliminary needed for fabrication of this biosensor following by its washing. Another PSA imprinted SPR biosensor was designed, using methacrylic acid and ethylene glycol dimethacrylate as a functional monomer and cross-linker, respectively [170]. This biosensor could detect PSA via SPR microcontact imprinting method in the range of 0.1 to 50 ng mL^{-1}, and the related LOD was 91 pg mL^{-1}. In this research, an imprinted chip was manufactured by microcontact imprinting technique and applied as a transducer. The obtained detection range and LOD were weaker than some other studies. In addition, employment of a nanostructure(s) would be improved the sensitivity and shortened the response time of this biosensor.

6. Conclusion

Given that the early diagnosis of prostate cancer is very important, various types of PSA biosensors were investigated in three main categories of aptasensors, peptisensors and immunosensors. Immunosensors have the disadvantages of time-consuming and expensive production, temperature sensitive and limited functionalization of the antibodies, and immunogenicity effects. In the aptasensors, rapid degradation by nucleases, renal filtration from bloodstream, interaction with some intracellular targets, and cross-reactivity of the aptamers are the limitations. Because the peptides can be selected from only known sequences, there are also some disadvantages for the peptisensors. The detection methods of the reviewed PSA biosensors were based on SERS, electrochemical, photoelectrochemical, fluorescence and chemiluminescence. Most of these biosensors have used different nanostructures to increase the sensitivity.

7. Perspectives

Functionalizing biodegradable components with materials that can form more stable bonds with the transducer as well as utilizing more efficient biorecognition elements in the structure of PSA biosensors can be one of outline of the future researches. It seems that the use of nanostructures as signal transducers, and biorecognition elements with high affinity, stability and specificity to bind PSA can propel the biosensors to higher sensitive diagnostic tools. Nanostructures with higher biocompatibility, greater stability and lower synthesis cost are favorable. Multiple biorecognition elements and multiple nanomaterials will allow simultaneous detection of multiple biomarkers; this would provide more comprehensive medical diagnosis routes. It is hoped that in

Table 3
Main details of PSA immunosensors.

Nanostructure	Detection technique	Detection range	LOD	Sensitivity	Specificity	Real sample type/ number	Ref.
Pt NPs	ECL	1.0 pg mL^{-1}-150 ng mL^{-1}	0.6 pg mL^{-1}	–	–	–	[91]
CdWS nanocrystals	ECL	0.0001–10 ng mL^{-1}	0.038 pg mL^{-1}	–	–	Serum/5	[77]
Pd@Au@Pt/COOH-rGO nanocomposites	ECL	3 pg mL^{-1}-60 ng mL^{-1}	2 pg mL^{-1}	0.099 μA ng mL^{-1}	–	Serum/5	[74]
CdS nanocrystals/Silica nanospheres	ECL	0.1 fg mL^{-1}-1 pg mL^{-1}	–	–	–	Serum/5	[92]
MWCNTs	ECL	2.25–11.3 ng mL^{-1}	0.88 ng mL^{-1}	–	–	Cell lysate/*	[93]
Pt NPs loaded on graphene sheets	ECL	1 pg mL^{-1}-10 ng mL^{-1}	0.3 pg mL^{-1}	–	97.3%	Serum/1	[78]
Au NPs@Bi_2S_3	ECL	0.005–5 ng mL^{-1}	3 pg mL^{-1}	–	–	Serum/1	[94]
MWCNTs/Nafion	ECL	0.1 pg mL^{-1}-20 ng mL^{-1}	35 fg mL^{-1}	–	97.4%	Serum/1	[95]
$EuPO_4$ nanowires	ECL	0.0005–80 ng mL^{-1}	177.33 fg mL^{-1}	–	–	Serum/1	[96]
Ag NPs	ECL	0.001–50 ng mL^{-1}	0.34 pg mL^{-1}	–	–	Serum/1	[97]
mpg-C_3N_4	ECL	0.001–15 ng mL^{-1}	0.927 pg mL^{-1}	–	–	Serum/1	[98]
Graphene QDs	ECL	1 pg mL^{-1}-10 ng mL^{-1}	0.29 pg mL^{-1}	–	–	Serum/1	[99]
Pt/Ag@BSA core–shell NPs	ECL	0.001–200 ng mL^{-1}	0.0003 ng mL^{-1}	–	–	Serum/5	[100]
Pd NPs	ECL	0.0001–50 ng mL^{-1}	0.056 pg mL^{-1}	–	98.6%	Serum/4	[79]
Fe_3O_4@MnO_2 nanocomposite	ECL	0.0001–10 ng mL^{-1}	5 fg mL^{-1}	–	–	Serum/1	[101]
QDs	Fluorescent	1–40 ng mL^{-1}	0.4 ng mL^{-1}	–	–	Serum/3	[102]
Silica nanospheres and Au@Ag NPs	Fluorescent	5 pg mL^{-1}-10 ng mL^{-1}	0.95 pg mL^{-1}	–	–	Serum/6	[103]
–	Fluorescent	0.1 pg mL^{-1}-10.269 ng mL^{-1}	0.1 pg mL^{-1}	0.027%	–	–	[104]
Nanomagnetic beads	Fluorescent	0.05–100 ng mL^{-1}	0.05 ng mL^{-1}	–	–	Serum/3	[80]
Graphene oxide QDs@Ag core–shell nanocrystals	Fluorescent	1 pg mL^{-1}-20 ng mL^{-1}	0.3 pg mL^{-1}	–	–	Serum/5	[105]
–	Fluorescent	0–10 ng mL^{-1}	1.2 ng mL^{-1}	10 pg mL^{-1}	–	Serum/1	[81]
CdTe QDs	Fluorescent	1–40 ng mL^{-1}	0.3 and 0.4 ng mL^{-1}	–	–	Serum/3	[102]
QDs	Fluorescence resonance energy transfer	0.01–100 ng mL^{-1}	1 pg mL^{-1}	–	–	Serum/4	[106]
–	SPR/Fluorescent	10 pmol L^{-1}-50 nmol L^{-1}	10 pM	–	–	–	[107]
CdSe/ZnS QDs/cysteine capped Mn-doped ZnS QDs	Phosphorescent	0.05–240 ng mL^{-1}	17 pg mL^{-1}	–	–	Serum/*	[83]
–	Chemiluminescence	0.02–125 ng mL^{-1}	0.007 ng mL^{-1}	–	–	Serum/40	[82]
–	Chemiluminescence	0.01 ng mL^{-1}-50 ng mL^{-1}	–	–	–	–	[49]
Hierarchical ZnO nanocolumns arrays	Photoluminescence	0–15 ng mL^{-1}	0.25 ng mL^{-1}	–	–	–	[108]
Ag NPs	SERS	0.001–1000 ng mL^{-1}	0.11 pg mL^{-1}	0.11 pg mL^{-1}	–	Serum/1	[89]
Au NPs	SERS	4–10 ng mL^{-1}	0.012 ng mL^{-1}	–	–	Serum/30	[90]
Au@1,4-benzenedithiol@Au core–shell	SERS	10 pg mL^{-1}-10 ng mL^{-1}	2 pg mL^{-1}	–	–	Serum/4	[109]
ZnO nanosphere/$CoFe_2O_4$@Au nanocomposite/Ag NPs	SERS	1 pg mL^{-1}-10 ng mL^{-1}	0.65 pg mL^{-1}	–	–	Serum/5	[110]
Metal organic frameworks	UV–vis	0.1–100 ng mL^{-1}	0.06 ng mL^{-1}	1.5mA ppb^{-1}	–	Serum/5	[111]
Iron oxide-to-prussian blue NPs	UV–vis	1–64 ng mL^{-1}	1 ng mL^{-1}	–	–	Serum/3	[112]
Mesoporous silica NPs	Colorimetric immunoassays	0.5–8000 pg mL^{-1}	0.36 pg mL^{-1}	–	–	–	[113]
Au NPs	Photoelectrochemical	1×10^{-11} g mL^{-1}-1.0×10^{-7} g mL^{-1}	2.7 pg mL^{-1}	–	–	Serum/9	[84]
SnS_2@mpg-C_3N_4 nanocomposite	Photoelectrochemical	50 fg mL^{-1}-10 ng mL^{-1}	21 fg mL^{-1}	–	–	Serum/3	[85]
ZnCdHgSe QDs and Au NRs	Photoelectrochemical	1 pg mL^{-1}-50 ng mL^{-1}	0.1 pg mL^{-1}	–	–	Serum/4	[114]
GO-Ca:CdSe nanocomposite	Photoelectrochemical	5 pg mL^{-1} – 50 ng mL^{-1}	2.6 pg mL^{-1}	–	–	Serum/1	[115]
CdS:Mn/g-C_3N_4 nanohybrids	Photoelectrochemical	0.01–20 ng mL^{-1}	3.8 pg mL^{-1}	–	–	Serum/6	[116]
Au NPs/CdS NRs	Photoelectrochemical	0.005–50 ng mL^{-1}	1.8 pg mL^{-1}	–	–	Serum/6	[117]
–	DPV	0.01–100 ng mL^{-1}	0.001 ng mL^{-1}	–	–	Serum/*	[118]
Au NPs/GO	DPV	0.001 fg mL^{-1}-0.02 μg mL^{-1}	5.4 fg mL^{-1}	5.4 μA fg mL^{-1}	–	Serum/1	[119]
TiO_2 NPs	DPV	0.10–5.0 ng mL^{-1}	200 pg mL^{-1}	–	5.62 μA	Serum/3	[120]
–	DPV	0.01–100 ng mL^{-1}	3 pg mL^{-1}	–	–	Serum/3	[121]
Au NPs/MWCNTs	DPV	15 pg mL^{-1}-8 ng mL^{-1}	1.7 pg mL^{-1}	–	–	–	[122]
Au NPs/GO	DPV	0.1 pg mL^{-1}-90 ng mL^{-1}	10 fg mL^{-1}	–	–	Serum/5	[48]
Au NPs/PdPtCu nanospheres	DPV	10 fg mL^{-1}-100 ng mL^{-1}	3.3 fg mL^{-1}	–	97%	Serum/4	[123]
Core-shell Au@Pt nanocrystals	DPV	0.1–50 ng mL^{-1}	0.018 ng mL^{-1}	–	–	Serum/1	[124]
Au NPs/MWNTs	DPV	10 pg mL^{-1}-100 ng mL^{-1}	5.4 pg mL^{-1}	–	–	Serum/3	[125]
CdTe@SiO_2 core–shell NPs/Fe_3O_4 NPs	DPV	0.01–5 ng mL^{-1}	0.003 ng mL^{-1}	–	–	Serum/4	[126]
Hydroxyl pillar[5]arene@Au NPs@g-C_3N_4 hybrid nanomaterial	DPV	0.0005–10 ng mL^{-1}	0.12 pg mL^{-1}	–	–	Serum/5	[127]
Au NPs	DPV/EIS	0.5 pg mL^{-1}-50 ng mL^{-1}	0.17 pg mL^{-1}	–	–	Serum/3	[128]
Au NPs/GO	DPV/EIS	0.003–1000 ng mL^{-1}	1 pg mL^{-1}	–	–	Serum/4	[129]
Au@mesoporous carbon nanocomposites	DPV/EIS	0.01–100 ng mL^{-1}	3 pg mL^{-1}	–	–	Serum/5	[130]
–	CV	up to 10 ng mL^{-1}	0.5 ng mL^{-1}	0.5 ng mL^{-1}	–	–	[131]
Au NPs	CV	0–100 ng mL^{-1}	7.8 ng mL^{-1}	–	–	–	[132]
Silica NPs	CV	4–10 ng ml^{-1}	2 pg mL^{-1}	4.9 μA ng^{-1} ml	83%	–	[133]

(*continued on next page*)

Table 3 (*continued*)

Nanostructure	Detection technique	Detection range	LOD	Sensitivity	Specificity	Real sample type/ number	Ref.
Nano Au	CV	10–50 fg mL^{-1}	4.7 fg mL^{-1}	–	–	–	[134]
AuPtAg alloyed nanocrystals	CV	0.05–50 ng mL^{-1}	0.017 ng mL^{-1}	–	–	Serum/*	[135]
–	CV/DPV	3.0–15.0 ng mL^{-1}	0.093 ng mL^{-1}	–	–	Serum/2	[136]
Au NPs-Poly(3,4-ethylenedioxythiophene)-graphene aerogel nanocomposite	CV/DPV/EIS	0.0001–50 ng mL^{-1}	0.03 pgmL^{-1}	–	–	Serum/4	[137]
rGO@Au NPs	CV/DPV/EIS	0.1–100 ng mL^{-1}	0.08 ng mL^{-1}	–	–	Serum/17	[138]
Core-shell AuPd@Au nanocrystals	CV/DPV/EIS	0.1–50 ng mL^{-1}	0.078 ng mL^{-1}	–	–	Serum/1	[139]
Mesoporous CeO_2/Au-CoS/graphene	CV/DPV/EIS	0.5 pg mL^{-1} –50 ng mL^{-1}	0.16 pg mL^{-1}	–	–	Serum/1	[140]
Gold-coated magnetic NPs	CV/EIS	0–25 ng mL^{-1}	0.085 ng mL^{-1}	–	–	Serum/4	[141]
Cu NPs	CV/EIS	0.01–100.0 ng mL^{-1}	0.003 ng mL^{-1}	–	–	Serum/3	[142]
Pd@Cu_2O/Au NPs	CV/EIS	0.0001–100 ng mL^{-1}	2 fg mL^{-1}	–	–	Serum/1	[143]
Pd NPs	CV/EIS	100 fg mL^{-1}-50 ng mL^{-1}	0.03 pg mL^{-1}	–	–	Serum/1	[144]
Au NPs	CV/EIS	1.0 fg mL^{-1}-100 ng mL^{-1}	0.09 fg mL^{-1}	973.01 Ω (lg(ng mL^{-1}))$^{-1}$	–	Serum/10	[145]
Pt-Cu hierarchical trigonal bipyramid nanoframes/GO	CV/EIS	0.0001–5 ng mL^{-1}	0.03 pgmL^{-1}	–	–	Serum/5	[146]
Au@Ag-Cu_2O NPs	CV/EIS	0.01 pg mL^{-1} –100 ng mL^{-1}	0.003 pg mL^{-1}	–	–	Serum/3	[147]
Au@thionine/GO nanocomposites	CV/EIS	50 fg mL^{-1}-40 ng mL^{-1}	16.6 fg mL^{-1}	–	–	Serum/1	[148]
Au NPs/GO	CV/EIS	0–10 ng mL^{-1}	0.59 ng mL^{-1}	–	–	–	[149]
Au NPs	CV/EIS	1–100 ng mL^{-1}	0.68 ng mL^{-1}	–	–	Serum/4	[150]
Pt NPs	CV/EIS	1–30 ng mL^{-1}	0.03 ng mL^{-1}	–	–	–	[151]
Graphene and Ag hybridized mesoporous silica	EIS	0.01–10 ng mL^{-1}	2 pg mL^{-1}	–	–	Serum/5	[152]
–	EIS	0.01–100 ng mL^{-1}	0.1 pg mL^{-1}	0.283 $mAng^{-1}$	–	–	[75]
Pd nano-octahedrons/MWCNTs	EIS	0.1 pg mL^{-1}-30 ng mL^{-1}	0.03 pg mL^{-1}	–	–	Serum/1	[153]
Cu_2O@CeO_2-Au nanocomposites	EIS	0.1 pg mL^{-1}-100 ng mL^{-1}	0.03 pg mL^{-1}	–	–	Serum/1	[154]
Pd@Pt-APTES-Cu_2O@Co_3O_4	EIS	0.01 pg mL^{-1}-100 ng mL^{-1}	2 fg mL^{-1}	–	–	Serum/3	[155]
–	EIS	100 ag mL^{-1}-1 μg mL^{-1}	100 ag mL^{-1}	–	–	Serum/6	[156]
Au NPs	EIS	1–500 ng mL^{-1}	1 ng mL^{-1}	–	–	–	[157]
Au NPs	SWV	0.2–200 ng mL^{-1}	0.01 ng mL^{-1}	–	–	–	[158]
Au NPs	SWV	0.1–50 ng mL^{-1}	0.08 ng mL^{-1}	–	–	Plasma/*	[159]
Au NPs	SWV/EIS/CV	1–18 ng mL^{-1}	0.001 ng mL^{-1}	–	–	Serum/1; urine/1; plasma/1	[160]
Halloysite nanotubes with polypyrrole shell and Pd NPs	SWV/EIS	0.0001–25 ng mL^{-1}	0.03 pg mL^{-1}	–	–	Serum/3	[161]
–	Bridge-shaped PZT resonator	10 pgmL^{-1}– 100 ng mL^{-1}	10 pgmL^{-1}	–	–	–	[162]
Au nanohole	Localized surface plasmon	0.3 pmol L^{-1}-3 nmol L^{-1}	140 fmol L^{-1}	–	–	–	[163]
Au NPs	Potentiometric	0.05–20 ng mL^{-1}	13.6 pg mL^{-1}	–	–	Serum/6	[164]
Graphene quantum/Au NPs	Chronoamperometry	2–9 pg mL^{-1}	1.8 pg mL^{-1}	–	–	Whole blood/1	[165]
–	Magnetic field sensing	0.1–10 ng mL^{-1}	0.1 ng mL^{-1}	–	–	–	[166]
Au NPs	Microfluidics real time electrochemical Profiling	0.2–25 ng mL^{-1}	0.2 ng mL^{-1}	–	–	–	[167]
–	ELISA	25–100 ng mL^{-1}	0.43 ng mL^{-1}	–	–	–	[168]

* The number of analyzed samples not reported.

the future, commercialization of PSA biosensors will be taken to be an effective step in the field of molecular diagnosis of prostate cancer.

Acknowledgments

We would like to thank the Research Council of Shiraz University of Medical Sciences (20907) for supporting this research.

References

[1] H. Grönberg, Lancet 361 (2003) 859.
[2] M.N. Bashir, Asian Pac. J. Cancer Prev. 16 (2015) 5137.
[3] G. Wu, R.H. Datar, K.M. Hansen, T. Thundat, R.J. Cote, A. Majumdar, Nat. Biotechnol. 19 (2001) 856.
[4] J.A. Saylor, L.B. Michaels, PSA and Prostate Cancer, Nova Science Publishers, 2010.
[5] A.M. Ward, J. Catto, F. Hamdy, Ann. Clin. Biochem. 38 (2001) 633.
[6] H. Graves, N. Wehner, T.A. Stamey, Clin. Chem. 38 (1992) 735.
[7] E. Johnson, T. Kotowski, J. Forensic Sci. 38 (1993) 250.
[8] C. Cao, J.P. Kim, B.W. Kim, H. Chae, H.C. Yoon, S.S. Yang, S.J. Sim, Biosens. Bioelectron. 21 (2006) 2106.
[9] F. Yu, B. Persson, S. Löfås, W. Knoll, Anal. Chem. 76 (2004) 6765.
[10] J. Tamayo, P.M. Kosaka, J.J. Ruz, Á. San Paulo, M. Calleja, Chem. Soc. Rev. 42 (2013) 1287.
[11] P.R. Solanki, A. Kaushik, V.V. Agrawal, B.D. Malhotra, NPG Asia Mater. 3 (2011) 17.
[12] R.D. Vais, N. Sattarahmady, H. Heli, Gold Bull. 49 (2016) 95.
[13] G. Tondro, R.D. Vais, N. Sattarahmady, Sens. Actuators, B 263 (2018) 36.
[14] L. Yang, X. Zhang, M. Ye, J. Jiang, R. Yang, T. Fu, Y. Chen, K. Wang, C. Liu, W. Tan, Adv. Drug Deliv. Rev. 63 (2011) 1361.
[15] H. Heli, M. Hajjizadeh, A. Jabbari, A. Moosavi-Movahedi, Anal. Biochem. 388 (2009) 81.
[16] N. Sattarahmady, H. Heli, A. Moosavi-Movahedi, Biosens. Bioelectron. 25 (2010) 2329.
[17] Y. Li, H.J. Schluesener, S. Xu, Gold Bull. 43 (2010) 29.
[18] Y.-Y. Lin, J. Wang, G. Liu, H. Wu, C.M. Wai, Y. Lin, Biosens. Bioelectron. 23 (2008) 1659.
[19] J.A. Hansen, J. Wang, A.-N. Kawde, Y. Xiang, K.V. Gothelf, G. Collins, J. Am. Chem. Soc. 128 (2006) 2228.
[20] L.M. Bellan, D. Wu, R.S. Langer, Wiley Interdiscip. Rev. Nanomed. Nanobiotechnol. 3 (2011) 229.

[21] C. Parolo, A. Merkoçi, Chem. Soc. Rev. 42 (2013) 450.
[22] M. Mascini, Aptamers and Their Applications, Springer, 2008.
[23] M. Ilgu, M. Nilsen-Hamilton, Analyst 141 (2016) 1551.
[24] J. Munkley, D.J. Elliott, Oncotarget 7 (2016) 35478.
[25] A. Díaz-Fernández, R. Miranda-Castro, N. de-los-Santos-Álvarez, E.F. Rodríguez, M.J. Lobo-Castañón, Biosens. Bioelectron. 128 (2019) 83.
[26] K. Yang, Y. Hu, N. Dong, G. Zhu, T. Zhu, N. Jiang, Biosens. Bioelectron. 94 (2017) 286.
[27] G. Cai, Z. Yu, R. Ren, D. Tang, ACS Sensors 3 (2018) 632.
[28] F. Qu, Y. Ding, X. Lv, L. Xia, J. You, W. Han, Anal. Bioanal. Chem. 411 (2019) 3979.
[29] R.-M. Kong, X. Zhang, L. Ding, D. Yang, F. Qu, Anal. Bioanal. Chem. 409 (2017) 5757.
[30] R.-M. Kong, L. Ding, Z. Wang, J. You, F. Qu, Anal. Bioanal. Chem. 407 (2015) 369.
[31] T. Cha, S. Cho, Y.T. Kim, J.H. Lee, Biosens. Bioelectron. 62 (2014) 31.
[32] P. Jolly, P. Zhurauski, J.L. Hammond, A. Miodek, S. Liébana, T. Bertok, J. Tkáč, P. Estrela, Sens. Actuators, B 251 (2017) 637.
[33] P. Miao, Y. Jiang, Y. Wang, J. Yin, Y. Tang, Sens. Actuators, B 257 (2018) 1021.
[34] T.T. Do, T. Van Phi, T.P. Nguy, P. Wagner, K. Eersels, C.V. Mun'delanji, L.T. Truong, J. Electron. Mater. 46 (2017) 3542.
[35] C.-Y. Lee, H.-T. Fan, Y.-Z. Hsieh, Sens. Actuators, B 255 (2018) 341.
[36] A. Raouafi, A. Sánchez, N. Raouafi, R. Villalonga, Sens. Actuators, B 297 (2019) 126762.
[37] Y. Zhu, H. Wang, L. Wang, J. Zhu, W. Jiang, ACS Appl. Mater. Interfaces 8 (2016) 2573.
[38] W. Argoubi, A. Sánchez, C. Parrado, N. Raouafi, R. Villalonga, Sens. Actuators, B 255 (2018) 309.
[39] N. Sattarahmady, A. Rahi, H. Heli, Sci. Rep. 7 (2017) 11238.
[40] A. Rahi, N. Sattarahmady, H. Heli, Talanta 156 (2016) 218.
[41] J.-T. Cao, J.-J. Yang, L.-Z. Zhao, Y.-L. Wang, H. Wang, Y.-M. Liu, S.-H. Ma, Biosens. Bioelectron. 99 (2018) 92.
[42] M. Souada, B. Piro, S. Reisberg, G. Anquetin, V. Noël, M. Pham, Biosens. Bioelectron. 68 (2015) 49.
[43] F. Tahmasebi, A. Noorbakhsh, Electroanalysis 28 (2016) 1134.
[44] P. Jolly, V. Tamboli, R.L. Harniman, P. Estrela, C.J. Allender, J.L. Bowen, Biosens. Bioelectron. 75 (2016) 188.
[45] E. Heydari-Bafrooei, N.S. Shamszadeh, Biosens. Bioelectron. 91 (2017) 284.
[46] B. Liu, L. Lu, E. Hua, S. Jiang, G. Xie, Microchim. Acta 178 (2012) 163.
[47] I. Tzouvadaki, P. Jolly, X. Lu, S. Ingebrandt, G. De Micheli, P. Estrela, S. Carrara, Nano Lett. 16 (2016) 4472.
[48] B. Kavosi, A. Salimi, R. Hallaj, F. Moradi, Biosens. Bioelectron. 74 (2015) 915.
[49] P. Jolly, P. Damborsky, N. Madaboosi, R.R. Soares, V. Chu, J.P. Conde, J. Katrlik, P. Estrela, Biosens. Bioelectron. 79 (2016) 313.
[50] W. Ma, H. Yin, L. Xu, X. Wu, H. Kuang, L. Wang, C. Xu, Chem. Commun. 50 (2014) 9737.
[51] T. Hao, X. Wu, L. Xu, L. Liu, W. Ma, H. Kuang, C. Xu, Small 13 (2017) 1603944.
[52] Z. Chen, Y. Lei, X. Chen, Z. Wang, J. Liu, Biosens. Bioelectron. 36 (2012) 35.
[53] B. Wei, K. Mao, N. Liu, M. Zhang, Z. Yang, Biosens. Bioelectron. 121 (2018) 41.
[54] P. Jolly, N. Formisano, J. Tkáč, P. Kasák, C.G. Frost, P. Estrela, Sens. Actuators, B 209 (2015) 306.
[55] B.P. Crulhas, A.E. Karpik, F.K. Delella, G.R. Castro, V.A. Pedrosa, Anal. Bioanal. Chem. 409 (2017) 6771.
[56] F. Zhang, S. Li, K. Cao, P. Wang, Y. Su, X. Zhu, Y. Wan, Sensors 15 (2015) 13839.
[57] A.B. Hughes, Amino Acids, Peptides and Proteins in Organic Chemistry, Analysis and Function of Amino Acids and Peptides, Wiley, 2013.
[58] A. Brajter-Toth, J. Chambers, Electroanalytical Methods of Biological Materials, CRC Press, 2002.
[59] G.M. Gersuk, M.J. Corey, E. Corey, J.E. Stray, G.H. Kawasaki, R.L. Vessella, Biochem. Biophys. Res. Commun. 232 (1997) 578.
[60] M. Negahdary, H. Heli, Biochem. Eng. J. 151 (2019) 107326.
[61] J.H. Choi, H.S. Kim, J.-W. Choi, J.W. Hong, Y.-K. Kim, B.-K. Oh, Biosens. Bioelectron. 49 (2013) 415.
[62] T. Feng, D. Feng, W. Shi, X. Li, H. Ma, Mol. BioSyst. 8 (2012) 1441.
[63] D. Wang, Y. Zheng, Y. Chai, Y. Yuan, R. Yuan, Chem. Commun. 51 (2015) 10521.
[64] Y. He, S. Xie, X. Yang, R. Yuan, Y. Chai, ACS Appl. Mater. Interfaces 7 (2015) 13360.
[65] S. Xie, J. Zhang, Y. Yuan, Y. Chai, R. Yuan, Chem. Commun. 51 (2015) 3387.
[66] I. Strzemińska, S.S.R. Fanchine, G. Anquetin, S. Reisberg, V. Noël, M. Pham, B. Piro, Biosens. Bioelectron. 81 (2016) 131.
[67] Z. Tang, Y. Fu, Z. Ma, Biosens. Bioelectron. 94 (2017) 394.
[68] H. Qi, M. Li, M. Dong, S. Ruan, Q. Gao, C. Zhang, Anal. Chem. 86 (2014) 1372.
[69] H. Qi, C. Wang, X. Qiu, Q. Gao, C. Zhang, Talanta 100 (2012) 162.
[70] X. Hun, Y. Xu, X. Luo, Microchim. Acta 182 (2015) 1669.
[71] A.M. Campbell, Monoclonal antibody and immunosensor technology: the production and application of rodent and human monoclonal antibodies, Elsevier, 1991.
[72] I. Vikholm, W. Albers, Langmuir 14 (1998) 3865.
[73] P. Karami, H. Bagheri, M. Johari-Ahar, H. Khoshsafar, F. Arduini, A. Afkhami, Talanta 202 (2019) 111.
[74] S. Barman, M. Hossain, H. Yoon, J.Y. Park, Biosens. Bioelectron. 100 (2018) 16.
[75] E. Cevik, Electroanalysis 31 (2019) 31.
[76] A.F. Quintero-Jaime, Á. Berenguer-Murcia, D. Cazorla-Amorós, E. Morallón, Front. Chem. 7 (2019).
[77] Q. Fang, Z. Lin, F. Lu, Y. Chen, X. Huang, W. Gao, Electrochim. Acta 302 (2019) 207.
[78] M.S. Khan, W. Zhu, A. Ali, S.M. Ahmad, X. Li, L. Yang, Y. Wang, H. Wang, Q. Wei, Anal. Biochem. 566 (2019) 50.
[79] L. Yang, Y. Li, Y. Zhang, D. Fan, X. Pang, Q. Wei, B. Du, ACS Appl. Mater. Interfaces 9 (2017) 35260.
[80] B. Li, J. Liu, H. Zhou, Anal. Chim. Acta 1008 (2018) 96.
[81] E. Takano, N. Shimura, Y. Ujima, H. Sunayama, Y. Kitayama, T. Takeuchi, ACS Omega 4 (2019) 1487.
[82] A. Liu, F. Zhao, Y. Zhao, L. Shangguan, S. Liu, Biosens. Bioelectron. 81 (2016) 97.
[83] M. García-Cortés, M.T. Fernández-Argüelles, J.M. Costa-Fernández, A. Sanz-Medel, Anal. Chim. Acta 987 (2017) 118.
[84] Y.-X. Dong, J.-T. Cao, Y.-M. Liu, S.-H. Ma, Biosens. Bioelectron. 91 (2017) 246.
[85] Y. Zhang, Y. Liu, R. Li, M.S. Khan, P. Gao, Y. Zhang, Q. Wei, Sci. Rep. 7 (2017) 4629.
[86] P. Karami, H. Khoshsafar, M. Johari-Ahar, F. Arduini, A. Afkhami, H. Bagheri, Spectrochim. Acta Part A Mol. Biomol. Spectrosc. (2019) 117218.
[87] S. Lv, K. Zhang, D. Tang, Analyst 144 (2019) 3716.
[88] Y. Wei, D. Wang, Y. Zhang, J. Sui, Z. Xu, Biosens. Bioelectron. 140 (2019) 111345.
[89] H. Chang, H. Kang, E. Ko, B.-H. Jun, H.-Y. Lee, Y.-S. Lee, D.H. Jeong, ACS Sensors 1 (2016) 645.
[90] Z. Cheng, N. Choi, R. Wang, S. Lee, K.C. Moon, S.-Y. Yoon, L. Chen, J. Choo, ACS Nano 11 (2017) 4926.
[91] X.-L. Huo, N. Zhang, J.-J. Xu, H.-Y. Chen, Electrochem. Commun. 98 (2019) 33.
[92] L. Deng, H.-Y. Chen, J.-J. Xu, Electrochem. Commun. 59 (2015) 56.
[93] A. Juzgado, A. Soldà, A. Ostric, A. Criado, G. Valenti, S. Rapino, G. Conti, G. Fracasso, F. Paolucci, M. Prato, J. Mater. Chem. B 5 (2017) 6681.
[94] J. Li, H. Ma, D. Wu, X. Li, Y. Zhao, Y. Zhang, B. Du, Q. Wei, Biosens. Bioelectron. 74 (2015) 104.
[95] Y. Liu, Y. Zhao, Z. Zhu, Z. Xing, H. Ma, Q. Wei, Anal. Chim. Acta 963 (2017) 17.
[96] H. Ma, J. Zhou, Y. Li, T. Han, Y. Zhang, L. Hu, B. Du, Q. Wei, Biosens. Bioelectron. 80 (2016) 352.
[97] H. Ma, X. Li, T. Yan, Y. Li, Y. Zhang, D. Wu, Q. Wei, B. Du, Biosens. Bioelectron. 79 (2016) 379.
[98] H. Ma, Y. Zhao, L. Li, H. Wang, Q. Wei, Talanta 188 (2018) 729.
[99] D. Wu, Y. Liu, Y. Wang, L. Hu, H. Ma, G. Wang, Q. Wei, Sci. Rep. 6 (2016) 20511.
[100] X. Xu, Bull. Korean Chem. Soc. 37 (2016) 452.
[101] W. Zhu, M.S. Khan, W. Cao, X. Sun, H. Ma, Y. Zhang, Q. Wei, Biosens. Bioelectron. 99 (2018) 346.
[102] Y. Chen, X. Guo, W. Liu, L. Zhang, Microchim. Acta 186 (2019) 112.
[103] J.-T. Cao, W.-S. Zhang, H. Wang, S.-H. Ma, Y.-M. Liu, New J. Chem. 43 (2019) 1424.
[104] J.-D. Li, J.-J. Cheng, B. Miao, X.-W. Wei, J. Xie, J.-C. Zhang, Z.-Q. Zhang, H.-W. Li, D.-M. Wu, Microsyst. Technol. 21 (2015) 1489.
[105] H. Pei, S. Zhu, M. Yang, R. Kong, Y. Zheng, F. Qu, Biosens. Bioelectron. 74 (2015) 909.
[106] B. Kavosi, A. Navaee, A. Salimi, J. Lumin. 204 (2018) 368.
[107] J. Breault-Turcot, H.-P. Poirier-Richard, M. Couture, D. Pelechacz, J.-F. Masson, Lab Chip 15 (2015) 4433.
[108] Y. Zou, Z. Huang, G. Yin, M. He, X. Liao, Nanosci. Nanotechnol. Lett. 8 (2016) 156.
[109] L. Wan, R. Zheng, J. Xiang, Vib. Spectrosc. 90 (2017) 56.
[110] L. Xie, X. Yang, Y. He, R. Yuan, Y. Chai, ACS Appl. Mater. Interfaces 10 (2018) 15200.
[111] S.K. Bhardwaj, A.L. Sharma, N. Bhardwaj, M. Kukkar, A.A. Gill, K.-H. Kim, A. Deep, Sens. Actuators, B 240 (2017) 10.
[112] G. Fu, S.T. Sanjay, X. Li, Analyst 141 (2016) 3883.
[113] F. Shao, L. Zhang, L. Jiao, X. Wang, L. Miao, H. Li, F. Zhou, Anal. Chem. 90 (2018) 8673.
[114] Y. Wang, X. Yu, X. Ye, K. Wu, T. Wu, C. Li, Anal. Chim. Acta 943 (2016) 106.
[115] X. Wang, R. Xu, X. Sun, Y. Wang, X. Ren, B. Du, D. Wu, Q. Wei, Biosens. Bioelectron. 96 (2017) 239.
[116] K. Zhang, S. Lv, Z. Lin, D. Tang, Biosens. Bioelectron. 95 (2017) 34.
[117] K. Zhang, S. Lv, Z. Lin, M. Li, D. Tang, Biosens. Bioelectron. 101 (2018) 159.
[118] E. Çevik, Ö. Bahar, M. Şenel, M.F. Abasıyanık, Biosens. Bioelectron. 86 (2016) 1074.
[119] M. Pal, R. Khan, Anal. Biochem. 536 (2017) 51.
[120] Z. Biniaz, A. Mostafavi, T. Shamspur, M. Torkzadeh-Mahani, M. Mohamadi, Microchim. Acta 184 (2017) 2731.
[121] L. Han, H. Xia, L. Yin, V.A. Petrenko, A. Liu, Biosens. Bioelectron. 106 (2018) 1.
[122] Y. Hao, P. Yan, X. Zhang, H. Shen, C. Gu, H. Zhang, M. Zhang, H. Xiang, Microchim. Acta 184 (2017) 4341.
[123] M. Li, P. Wang, F. Pei, H. Yu, Y. Dong, Y. Li, Q. Liu, P. Chen, Sens. Actuators, B 261 (2018) 22.
[124] R. Wang, A.-J. Wang, W.-D. Liu, P.-X. Yuan, Y. Xue, X. Luo, J.-J. Feng, Biosens. Bioelectron. 102 (2018) 276.
[125] J. Yang, W. Wen, X. Zhang, S. Wang, Microchim. Acta 182 (2015) 1855.
[126] Y. Zhao, W. Gao, X. Ge, S. Li, D. Du, H. Yang, Anal. Chim. Acta 1057 (2019) 44.
[127] X. Zhou, L. Yang, X. Tan, G. Zhao, X. Xie, G. Du, Biosens. Bioelectron. 112 (2018) 31.
[128] J. Guo, J. Wang, J. Zhao, Z. Guo, Y. Zhang, ACS Appl. Mater. Interfaces 8 (2016) 6898.
[129] M. Karimipour, E. Heydari-Bafrooei, M. Sanjari, M.B. Johansson, M. Molaei, Microchim. Acta 186 (2019) 33.
[130] L. Yang, H. Zhao, G. Deng, X. Ran, Y. Li, X. Xie, C.-P. Li, RSC Adv. 5 (2015) 74046.
[131] J. Zapatero-Rodríguez, S. Liébana, S. Sharma, S. Gilgunn, G.A. Drago, R. O'Kennedy, BioNanoScience 8 (2018) 680.
[132] D. Kiziltan, T. Vural, C. Bayram, S. Ozturk, B. Bozdogan, Y.T. Yaman, S. Abaci, E.B. Denkbas, Anal. Sci. 34 (2018) 789.
[133] S. Rafique, W. Bin, A.S. Bhatti, Bioelectrochemistry 101 (2015) 75.

[134] S. Rawlinson, P. Kanyong, A. McConville, J.-J. Fearon, J.A. McLaughlin, J. Davis, Chem. Lett. 46 (2017) 1728.
[135] Y.-C. Shi, A.-J. Wang, P.-X. Yuan, L. Zhang, X. Luo, J.-J. Feng, Biosens. Bioelectron. 111 (2018) 47.
[136] T. Shamspur, Z. Biniaz, A. Mostafavi, M. Torkzadeh-Mahani, M. Mohamadi, IEEE Sens. J. 18 (2018) 4861.
[137] H. Jia, J. Xu, L. Lu, Y. Yu, Y. Zuo, Q. Tian, P. Li, Sens. Actuators, B 260 (2018) 990.
[138] X. Liu, D. Wang, J. Chu, Y. Xu, W. Wang, J. Pharm. Biomed. Anal. 158 (2018) 361.
[139] R. Wang, W.-D. Liu, A.-J. Wang, Y. Xue, L. Wu, J.-J. Feng, Biosens. Bioelectron. 99 (2018) 458.
[140] Y. Wei, X. Li, X. Sun, H. Ma, Y. Zhang, Q. Wei, Biosens. Bioelectron. 94 (2017) 141.
[141] H. Hwang, E. Choi, S. Han, Y. Lee, T. Choi, M. Kim, H. Shin, J. Kim, J. Choi, Anal. Chim. Acta 1061 (2019) 92.
[142] Y. Chen, P.-X. Yuan, A.-J. Wang, X. Luo, Y. Xue, L. Zhang, J.-J. Feng, Biosens. Bioelectron. 126 (2019) 187.
[143] Y. Chu, H. Wang, H. Ma, D. Wu, B. Du, Q. Wei, RSC Adv. 6 (2016) 84698.
[144] L. Dai, Y. Li, Y. Wang, X. Luo, D. Wei, R. Feng, T. Yan, X. Ren, B. Du, Q. Wei, Biosens. Bioelectron. 132 (2019) 97.
[145] L. Zhao, S. Yin, Z. Ma, ACS Sens 4 (2019) 450.
[146] L. Jiao, Z. Mu, L. Miao, W. Du, Q. Wei, H. Li, Microchim. Acta 184 (2017) 423.
[147] Y. Yang, Q. Yan, Q. Liu, Y. Li, H. Liu, P. Wang, L. Chen, D. Zhang, Y. Li, Y. Dong, Biosens. Bioelectron. 99 (2018) 450.
[148] J. Feng, Y. Li, M. Li, F. Li, J. Han, Y. Dong, Z. Chen, P. Wang, H. Liu, Q. Wei, Biosens. Bioelectron. 91 (2017) 441.
[149] H.D. Jang, S.K. Kim, H. Chang, J.-W. Choi, Biosens. Bioelectron. 63 (2015) 546.
[150] T. Vural, Y.T. Yaman, S. Ozturk, S. Abaci, E.B. Denkbas, J. Colloid Interface Sci. 510 (2018) 318.
[151] E. Spain, S. Gilgunn, S. Sharma, K. Adamson, E. Carthy, R. O'Kennedy, R.J. Forster, Biosens. Bioelectron. 77 (2016) 759.
[152] Y. Li, J. Han, R. Chen, X. Ren, Q. Wei, Anal. Biochem. 469 (2015) 76.
[153] L. Liu, Y. Li, L. Tian, Q. Wei, W. Cao, Sens. Actuators, B 237 (2016) 733.
[154] F. Li, Y. Li, J. Feng, Y. Dong, P. Wang, L. Chen, Z. Chen, H. Liu, Q. Wei, Biosens. Bioelectron. 87 (2017) 630.
[155] L. Liu, G. Zhao, X. Dong, X. Li, Q. Wei, W. Cao, Anal. Methods 10 (2018) 4917.
[156] D. Pihikova, P. Kasak, P. Kubanikova, R. Sokol, J. Tkac, Anal. Chim. Acta 934 (2016) 72.
[157] C. Rodriguez, V. Torres-Costa, O. Ahumada, V. Cebrian, C. Gomez-Abad, A. Diaz, M.M. Silván, Sens. Actuators, B 267 (2018) 559.
[158] N. Oliveira, E. Costa-Rama, S. Viswanathan, C. Delerue-Matos, L. Pereira, S. Morais, Electroanalysis 30 (2018) 2604.
[159] L. Talamini, N. Zanato, E. Zapp, D. Brondani, E. Westphal, H. Gallardo, I.C. Vieira, Electroanalysis 30 (2018) 353.
[160] L. Suresh, P.K. Brahman, K.R. Reddy, B. JS, Enzyme Microbial Technol. 112 (2018) 43.
[161] Y. Li, M.S. Khan, L. Tian, L. Liu, L. Hu, D. Fan, W. Cao, Q. Wei, Anal. Bioanal. Chem. 409 (2017) 3245.
[162] D.G. Hwang, Y.M. Chae, N. Choi, I.-J. Cho, J.Y. Kang, S.H. Lee, Microsyst. Technol. 23 (2017) 1207.
[163] Q. Zhang, L. Wu, J.Z. Ten It Wong, X. Liu, X. Zhou, P. Bai, B. Liedberg, Y. Wang, Int. J. Nanomed. 12 (2017) 2307.
[164] S. Lv, Z. Lin, K. Zhang, M. Lu, D. Tang, Anal. Chim. Acta 964 (2017) 67.
[165] H. Malekzad, M. Hasanzadeh, N. Shadjou, A. Jouyban, Int. J. Biol. Macromol. 105 (2017) 522.
[166] X.-C. Sun, C. Lei, L. Guo, Y. Zhou, Microchim. Acta 183 (2016) 2385.
[167] Y. Uludag, G. Köktürk, Microchim. Acta 182 (2015) 1685.
[168] G.G. Gutiérrez-Zúñiga, J.L. Hernández-López, Anal. Chim. Acta 902 (2016) 97.
[169] Z. Yazdani, H. Yadegari, H. Heli, Anal. Biochem. 566 (2019) 116.
[170] G. Ertürk, H. Özen, M.A. Tümer, B. Mattiasson, A. Denizli, Sens. Actuators, B 224 (2016) 823.